Geosci. Model Dev. Discuss., 8, 2555–2603, 2015
www.geosci-model-dev-discuss.net/8/2555/2015/
doi:10.5194/gmdd-8-2555-2015

Geoscientific Model Development Discussions
Open Access

A non-equilibrium model for soil heating and moisture transport during extreme surface heating

W. J. Massman

USDA Forest Service, Rocky Mountain Research Station, 240 West Prospect, Fort Collins, CO 80526, USA

Received: 4 February 2015 – Accepted: 21 February 2015 – Published: 6 March 2015

Correspondence to: W. J. Massman (wmassman@fs.fed.us)

Published by Copernicus Publications on behalf of the European Geosciences Union.

Abstract

With increasing use of prescribed fire by land managers and increasing likelihood of wildfires due to climate change comes the need to improve modeling capability of extreme heating of soils during fires. This issue is addressed here by developing a one-dimensional non-equilibrium model of soil evaporation and transport of heat, soil moisture, and water vapor, for use with surface forcing ranging from daily solar cycles to extreme conditions encountered during fires. The model employs a linearized Crank–Nicolson scheme for the conservation equations of energy and mass and its performance is evaluated against dynamic soil temperature and moisture observations obtained during laboratory experiments on soil samples exposed to surface heat fluxes ranging between 10 000 and 50 000 W m^{-2}. The Hertz–Knudsen equation is the basis for constructing the model's non-equilibrium evaporative source term. The model includes a dynamic residual soil moisture as a function of temperature and soil water potential, which allows the model to capture some of the dynamic aspects of the strongly bound soil moisture that seems to require temperatures well beyond 150 °C to fully evaporate. Furthermore, the model emulates the observed increase in soil moisture ahead of the drying front and the hiatus in the soil temperature rise during the strongly evaporative stage of drying. It also captures the observed rapid evaporation of soil moisture that occurs at relatively low temperatures (50–90 °C). Sensitivity analyses indicate that the model's success results primarily from the use of a temperature and moisture potential dependent condensation coefficient in the evaporative source term. The model's solution for water vapor density (and vapor pressure), which can exceed one standard atmosphere, cannot be experimentally verified, but they are supported by results from (earlier and very different) models developed for somewhat different purposes and for different porous media. Overall, this non-equilibrium model provides a much more physically realistic simulation over a previous equilibrium model developed for the same purpose. Current model performance strongly suggests that it is now ready for testing under field conditions.

GMDD
8, 2555–2603, 2015

1 Introduction

Since the development of the theory of Philip and de Vries (PdV model) almost 60 years ago (Philip and de Vries, 1957; de Vries, 1958) virtually all models of evaporation and condensation in unsaturated soils have assumed that soil water vapor at any particular depth into the soil is in equilibrium with the liquid soil water (or soil moisture) at the same depth. In essence, this local equilibrium assumption means that whenever the soil moisture changes phase it does so instantaneously. But for modeling purposes it also means a significant simplification to the equations that describe heat and moisture flow in soils because it eliminates the need to include soil water vapor density, ρ_v, as an independent model variable. Rather ρ_v is directly equated to the equilibrium vapor density, which is a function only of local soil temperature and soil water content (or more specifically the soil water potential). The original motivation for this model was to describe the coupled heat and moisture transport in soils (and soil evaporation in particular) under environmental forcings associated with the daily and seasonal variations in radiation, temperature, precipitation, etc. (e.g., Milly, 1982; Novak, 2010; Smits et al., 2011). Since the time of the original PdV model the equilibrium assumption has been incorporated into models of heat and moisture transport (evaporation and condensation) in soils and other porous media under more extreme forcings associated with high temperatures and heat fluxes. For example, it has been applied to (i) soils during wildfires and prescribed burns (Aston and Gill, 1976; Campbell et al., 1995; Durany et al., 2010; Massman, 2012), (ii) drying of wood (Whitaker, 1977; di Blasi, 1997), (iii) drying and fracturing of concrete under high temperatures (Dayan, 1982; Dal Pont et al., 2011), (iv) high temperature sand-water-steam systems (e.g., Udell, 1983; Bridge et al., 2003), and (v) evaporation of wet porous thermal barriers under high heat fluxes (Costa et al., 2008).

Although the PdV model and the equilibrium assumption have certainly lead to many insights into moisture and vapor transport and evaporation in porous media, it has, nonetheless, yielded somewhat disappointing simulations of the coupled soil moisture

GMDD
8, 2555–2603, 2015

dynamics during fires (see Massman, 2012 for further details and general modeling review). Possibly the most interesting of these modeling "disappointments" is provided by soil/fire-heating model of Massman (2012), who found that as the soil moisture evaporated it just re-condensed and accumulated ahead of the dry zone, so that no water actually escaped the soil at all (which, to say the least, seems physically implausible)! He further suggested that one possible cause for this failure is the inapplicability of the equilibrium evaporation assumption. There is some support for this supposition. Certainly the equilibrium assumption is likely to fail under extremely dry conditions, (e.g., Novak, 2012), which are guaranteed to occur during extreme heating events like fires. In addition, the modeling results of both Smits et al. (2011) and Ouedraogo et al. (2013) suggest that non-equilibrium formulations of soil evaporation improve model performance (over the equilibrium approach) under the less extreme environmental forcing that is typical near the earth's surface. Otherwise to the author's knowledge Massman's (2012) non-equilibrium hypothesis has never been tested during extreme conditions. The present study is intended to provide the first such test.

Specifically, the present study develops and evaluates a non-equilibrium model for simulating coupled heat, moisture, and water vapor transport during extreme heating events. It uses a systems-theoretic approach (e.g., Gupta and Nearing, 2014) focused more on physical processes than simply tuning model parameters, which here means that whatever model or parameter "tuning" does occur it is intended to keep the model numerically stable and as physically realistic as possible.

In addition, the present study (model) is a companion to Massman (2012). It uses much of the same notation as the earlier study. And it also improves on and corrects (where possible and as noted in the text) the mathematical expressions used in the previous paper to parameterize the high temperature dependency of latent heat of vaporization, saturation vapor density, diffusivity of water vapor, soil thermal conductivity, water retention curve, etc. And lastly, in order to facilitate comparing the present model with the earlier companion model the present study displays all graphical results in a manner very similar to those of Massman's (2012).

GMDD
8, 2555–2603, 2015

2 Model development

The present model is one-dimensional (in the vertical) and is developed from three coupled partial differential equations and assumes that soil evaporation is a non-equilibrium process. Consequently the present model has three simulation variables: soil temperature ($\equiv T$ [C] or T_K [K]); soil water potential ($\equiv \psi$ [J kg^{-1}] or $\psi_n \equiv$ normalized soil water potential (*dimensionless*), where $\psi_n = \psi/\psi_*$ and $\psi_* = -10^6$ [J kg^{-1}], which Campbell et al. (1995) identify as the water potential for oven dry soil); and vapor density ($\equiv \rho_v$ [kg m^{-3}]), which is not explicitly modeled with equilibrium models. This current model employs a linearized Crank–Nicolson (C-N) finite difference scheme, whereas the preceding (companion) model (Massman, 2012) used the Newton–Raphson method for solving the fully implicit finite difference equations. The present model further improves on its companion by including the possibility of soil water movement (hydraulic conductivity function driven by a gradient in soil moisture potential) and better parameterizations of thermophysical properties of water and water vapor to allow for large variations in the amount of soil water vapor, which Massman's (2012) results suggest might approach or exceed one standard atmosphere and therefore could become the major component of the soil atmosphere during a heating event. This is quite unlike any other model of soil heat and moisture flow, which universally assume that dry air is the dominant component of the soil atmosphere and that water vapor is a relatively minor component. Finally, and also atypical of most other soil models, the model's water retention curve and hydraulic function include a dynamic residual soil moisture content as a function of soil temperature and soil water potential.

2.1 Conservation equations

The conservation of thermal energy is expressed as:

$$C_s \frac{\partial T}{\partial t} - \frac{\partial}{\partial z}\left[\lambda_s \frac{\partial T}{\partial z}\right] + (\eta - \theta)\rho_a c_{pa} u_{vl} \frac{\partial T}{\partial z} = -L_v S_v \quad (1)$$

GMDD
8, 2555–2603, 2015

where t [s] is time; z [m] is soil depth (positive downward); T is soil temperature in °C; $C_s = C_s(\theta, T)$ [J m^{-3} K^{-1}] is the volumetric heat capacity of soil, a function of both soil temperature and soil volumetric water content θ [m^3 m^{-3}]; $\lambda_s = \lambda_s(\theta, T, \rho_v)$ [W m^{-1} K^{-1}] is the thermal conductivity of the soil, a function of soil temperature, soil moisture, and soil vapor density; η [m^3 m^{-3}] is the total soil porosity from which it follows that $(\eta - \theta)$ is the soil's air filled porosity; $\rho_a = \rho_a(T_K, \rho_v)$ [kg m^{-3}] is the mass density of the soil air, a function of temperature and soil vapor density; $c_{pa} = c_{pa}(T_K, \rho_v)$ [J kg^{-1} K^{-1}] is specific heat capacity of ambient air, also a function of temperature and vapor density; u_{vl} [m s^{-1}] is the advective velocity induced by the change in volume associated with the rapid volitalization of soil moisture (detailed below); $L_v = L_v(T_K, \psi)$ [J kg^{-1}] is the latent heat of vaporization; and $S_v = S_v(T_K, \theta, \psi, \rho_v)$ [kg m^{-3} s^{-1}] is the source term for water vapor.

The conservation of mass for liquid water is

$$\frac{\partial(\rho_w \theta)}{\partial t} - \frac{\partial}{\partial z}\left[\rho_w \mathcal{K}_n \frac{\partial \psi_n}{\partial z} + \rho_w \mathcal{K}_H - \rho_w V_{\theta,surf}\right] = -S_v \tag{2}$$

$\rho_w = \rho_w(T_K)$ [kg m^{-3}] is the density of liquid water; $\mathcal{K}_n = \mathcal{K}_n(T_K, \theta)$ [m^2 s^{-1}] is the "normalized" hydraulic conductivity; $\mathcal{K}_H = \mathcal{K}_H(T_K, \theta)$ [m s^{-1}] is the "hydraulic conductivity"; and $V_{\theta,surf} = V_{\theta,surf}(T_K, \theta)$ [m s^{-1}] is the velocity of liquid water associated with surface diffusion of water, which may be significant at high temperatures (e.g., Kapoor et al., 1989; Medved and Černý, 2011). Note that switching variables from $\psi < 0$, to ψ_n produces $\psi_n > 0$ and $\mathcal{K}_n < 0$.

This last equation can be simplified to

$$\rho_w \frac{\partial \theta}{\partial t} - \rho_w \frac{\partial}{\partial z}\left[\mathcal{K}_n \frac{\partial \psi_n}{\partial z} + \mathcal{K}_H - V_{\theta,surf}\right] = -S_v \tag{3}$$

because $\frac{1}{\rho_w}\frac{d\rho_w}{dT}$ varies by only 4 % between about 10 to 100 °C the derivatives $\frac{\partial \rho_w}{\partial t} \equiv \frac{d\rho_w}{dT}\frac{\partial T}{\partial t}$ and $\frac{\partial \rho_w}{\partial z} \equiv \frac{d\rho_w}{dT}\frac{\partial T}{\partial z}$ can be ignored. But the model does retain the temperature

GMDD
8, 2555–2603, 2015

dependency $\rho_w = \rho_w(T_K)$, except as noted in the section below on volumetric specific heat capacity of soil, and it also specifically includes $d\rho_w/dT$ for other components of the model.

The conservation of mass for water vapor is

$$\frac{\partial(\eta-\theta)\rho_v}{\partial t} - \frac{\partial}{\partial z}\left[D_{ve}\frac{\partial \rho_v}{\partial z} - (\eta-\theta)u_{vl}\rho_v\right] = S_v \quad (4)$$

where $D_{ve} = D_{ve}(T_K, \psi, \rho_v)$ [$m^2\,s^{-1}$] is the (equivalent) molecular diffusivity associated with the diffusive transport of water vapor in the soil's air-filled pore space.

The final model equations are expressed in terms of the model variables (T, ψ_n, ρ_v) and result from: (a) expanding the spatial derivative $\frac{\partial \mathcal{K}_H}{\partial z}$ in terms of the spatial derivatives $\frac{\partial T}{\partial z}$ and $\frac{\partial \psi_n}{\partial z}$, (b) allowing for $\theta = \theta(\psi_n, T_K)$, (c) combining Eq. (3) with Eq. (1) and Eq. (4) with Eq. (3), and (d) simplifying Eq. (4). These equations are

$$(C_s - L_v\rho_w D_{\theta T})\frac{\partial T}{\partial t} - \frac{\partial}{\partial z}\left[\lambda_s\frac{\partial T}{\partial z}\right] + \left[(\eta-\theta)\rho_a c_{pa}u_{vl} + L_v\rho_w\frac{\delta \mathcal{K}_H}{\delta T_K}\right]\frac{\partial T}{\partial z}$$
$$+ L_v\rho_w\frac{\partial}{\partial z}\left[\mathcal{K}_m\frac{\partial T}{\partial z}\right] - L_v\rho_w D_{\theta\psi}\frac{\partial \psi_n}{\partial t} + L_v\rho_w\frac{\partial}{\partial z}\left[\mathcal{K}_n^*\frac{\partial \psi_n}{\partial z}\right] + L_v\rho_w\left[\frac{\partial \mathcal{K}_H}{\partial \psi_n}\right]\frac{\partial \psi_n}{\partial z} = 0 \quad (5)$$

which is the conservation of energy;

$$\rho_w D_{\theta T}\frac{\partial T}{\partial t} - \rho_w\frac{\partial}{\partial z}\left[\mathcal{K}_m\frac{\partial T}{\partial z}\right] - \rho_w\left[\frac{\delta \mathcal{K}_H}{\delta T_K}\right]\frac{\partial T}{\partial z} + \rho_w D_{\theta\psi}\frac{\partial \psi_n}{\partial t} - \rho_w\frac{\partial}{\partial z}\left[\mathcal{K}_n^*\frac{\partial \psi_n}{\partial z}\right]$$
$$- \rho_w\left[D_{\theta\psi}\frac{\partial \mathcal{K}_H}{\partial \theta}\right]\frac{\partial \psi_n}{\partial z} + (\eta-\theta)\frac{\partial \rho_v}{\partial t} - \frac{\partial}{\partial z}\left[\mathcal{D}_v\frac{\partial \rho_v}{\partial z} - (\eta-\theta)u_{vl}\rho_v\right] = 0 \quad (6)$$

which is the conservation of soil moisture; and

$$-\rho_v D_{\theta T}\frac{\partial T}{\partial t} + (\eta-\theta)\frac{\partial \rho_v}{\partial t} - \frac{\partial}{\partial z}\left[\mathcal{D}_v\frac{\partial \rho_v}{\partial z} - (\eta-\theta)u_{vl}\rho_v\right] - \rho_v D_{\theta\psi}\frac{\partial \psi_n}{\partial t} = S_v \quad (7)$$

GMDD
8, 2555–2603, 2015

which is the conservation of mass for water vapor.

Apropos to these last three equations: (i) $D_{\theta\psi} = \partial\theta/\partial\psi_n$ and $D_{\theta T} = \partial\theta/\partial T_K$ are obtained from the water retention curve (WRC), (ii) $\frac{\delta\mathcal{K}_H}{\delta T_K} = \left[\frac{\partial\mathcal{K}_H}{\partial T_K} + \frac{\partial\mathcal{K}_H}{\partial\theta}D_{\theta T}\right]$, (iii) $\mathcal{K}_m$ [$m^2\,s^{-1}\,K^{-1}$] and $\mathcal{K}^*_n$ [$m^2\,s^{-1}$] (which subsumes $\mathcal{K}_n$) are related to $V_{\theta,surf}$ and are defined in a later section, (iv) because $\rho_v \ll \rho_w$ the term $(\rho_w - \rho_v)\frac{\partial\theta}{\partial t}$ originally in Eq. (6) has been approximated by $\rho_w\frac{\partial\theta}{\partial t} \equiv \rho_w D_{\theta\psi}\frac{\partial\psi_n}{\partial t} + \rho_w D_{\theta T}\frac{\partial T}{\partial t}$; and (v) the total porosity η is assumed to be spatially uniform and temporally invariant.

2.2 Functional parameterizations

2.2.1 Thermophysical properties of water, vapor, and moist air

The algorithm for calculating water density, $\rho_w(T_K)$, is Eq. (2.6) of Wagner and Pruess (2002) and employed only within the temperature range $273.15\,K \le T_K \le 383.15\,K$ ($\equiv T_{K,max}$). At temperatures greater than $T_{K,max}$, then $\rho_w(T_K) = \rho_w(T_{K,max})$. This approach yields a range for $\rho_w(T_K)$ of $950\,kg\,m^{-3} < \rho_w(T_K) < 1000\,kg\,m^{-3}$, which represents a compromise between the fact that the density of (free saturated liquid) water continues to decrease with increasing temperatures (Yaws, 1995) and the possibility that in a bound state a mono-layer of liquid water $\rho_w(T_K)$ may reach values as high as $\approx 5000\,kg\,m^{-3}$ (Danielewicz-Ferchmin and Mickiewicz, 1996). $d\rho_w/dT$ is computed from the analytical expression derived by differentiating the expression for $\rho_w(T_K)$ and $d\rho_w/dT = 0$ for $T_K > T_{K,max}$.

The enthalpy of vaporization of water, $H_v = H_v(T_K, \psi)$ [$J\,mol^{-1}$], is Eq. (5) of Somayajulu (1988) augmented by the soil moisture potential, ψ, (Massman, 2012; Campbell et al., 1995) and is expressed as follows:

$$H_v = H_1\left(\frac{T_{crit} - T_K}{T_K}\right) + H_2\left(\frac{T_{crit} - T_K}{T_{crit}}\right)^{\frac{3}{8}} + H_3\left(\frac{T_{crit} - T_K}{T_{crit}}\right)^{\frac{9}{4}} - M_w\psi \quad (8)$$

GMDD
8, 2555–2603, 2015

where $H_1 = 13.405538\,\mathrm{kJ\,mol^{-1}}$, $H_2 = 54.188028\,\mathrm{kJ\,mol^{-1}}$, $H_3 = -58.822461\,\mathrm{kJ\,mol^{-1}}$, $T_{crit} = 647.096\,\mathrm{K}$ is the critical temperature for water, and $M_w = 0.01802\,\mathrm{kg\,mol^{-1}}$ is the molar mass of water vapor. Note that $h_v = h_v(T_K)$ [$\mathrm{J\,mol^{-1}}$] will denote the enthalpy of vaporization without the additional $-M_w\psi$ term, i.e., $h_v = h_v(T_K) = H_1(T_{crit} - T_K)/T_K + H_2[(T_{crit} - T_K)/T_{crit}]^{\frac{3}{8}} + H_3[(T_{crit} - T_K)/T_{crit}]^{\frac{9}{4}}$. The present formulation differs from Massman (2012) because here $h_v(T_K \geq T_{crit}) = 0$; whereas Massman's (and Campbell's et al., 1995) equivalent h_v was a linear approximation of the present h_v, which yielded $h_v(T_K \geq T_{crit}) \gg 0$. This distinction will become important when discussing the water vapor source term, S_v. Note that because $L_v = H_v/M_w$ it also employs Eq. (8).

The formulations for thermal conductivity of water vapor, $\lambda_v = \lambda_v(T_K)$ [$\mathrm{W\,m^{-1}\,K^{-1}}$], and liquid water, $\lambda_w = \lambda_w(T_K, \rho_w)$ [$\mathrm{W\,m^{-1}\,K^{-1}}$], are taken from Huber et al. (2012). For water vapor their Eq. (4) is used and for liquid water the product of their Eqs. (4) and (5) is used. The formulations for viscosity of water vapor and liquid water are taken from Huber et al. (2009) and are similar algorithmically to thermal conductivity. For water vapor, $\mu_v = \mu_v(T_K)$ [$\mathrm{kg\,m^{-1}\,s^{-1}} \equiv \mathrm{Pa\,s}$], their Eq. (11) is used and for liquid water, $\mu_w = \mu_w(T_K, \rho_w)$ [Pa s], their Eq. (36) is used. For liquid water both these formulations include a dependence on the density of water. Consequently, once soil temperature exceeds $T_{K,max}$ both λ_w and μ_w are assigned a fixed value determined at $T_{K,max}$. On the other hand, λ_v and μ_v increase continually with increasing temperatures.

The formulation for the thermal conductivity of dry air, $\lambda_d = \lambda_d(T_K)$ [$\mathrm{W\,m^{-1}\,K^{-1}}$], is Eq. (5a) of Kadoya et al. (1985) and for the viscosity of dry air, $\mu_d = \mu_d(T_K)$ [Pa s], Eq. (3a) of Kadoya et al. (1985) is used. The model of the thermal conductivity of soil atmosphere, $\lambda_a = \lambda_a(\lambda_v, \lambda_d, \mu_v, \mu_d)$ [$\mathrm{W\,m^{-1}\,K^{-1}}$], is a non-linear expression given by Eq. (28) of Tsilingiris (2008). The relative weights used in this formulation are determined using the mixing ratios for water vapor (χ_v (dimensionless)) and dry air ($\chi_d = 1 - \chi_v$): where $\chi_v = e_v/(P_d + e_v)$, e_v [Pa] is the vapor pressure, and P_d [Pa] is the dry air pressure. Here P_d will be held constant and equal to the ambient atmospheric pressure, P_{atmos} [$= 92\,\mathrm{kPa}$], during the laboratory experiments (see Massman, 2012;

GMDD
8, 2555–2603, 2015

Campbell et al., 1995). The vapor pressure, e_v, is obtained from ρ_v and T_K using the ideal gas law.

The volumetric specific heat for soil air, $\rho_a c_{pa}$ [$J\,m^{-3}\,K^{-1}$], is estimated for the soil atmosphere from $\rho_a c_{pa} = c_{pv}\rho_v + c_{pd}\rho_d$; where $\rho_d = M_d P_{atmos}/(RT_K)$ [$kg\,m^{-3}$] is the dry air density, $R = 8.314\,J\,mol^{-1}\,K^{-1}$ is the universal gas constant, $M_d = 0.02896\,kg\,mol^{-1}$ is the molar mass of dry air, and the isobaric specific heats for water vapor, c_{pv} [$J\,kg^{-1}\,K^{-1}$], and dry air, c_{pd} [$J\,kg^{-1}\,K^{-1}$], use Eq. (6) of Bücker et al. (2003).

The saturation vapor pressure, $e_{v,\,sat} = e_{v,\,sat}(T_K)$ [Pa], and its derivative, $de_{v,\,sat}/dT$ [$Pa\,K^{-1}$], are modeled using Eqs. (2.5) and (2.5a) of Wagner and Pruess (2002). The saturation vapor density, $\rho_{v,\,sat}$ [$kg\,m^{-3}$], is modeled using Eq. (2.7) of Wagner and Pruess (2002). Following Massman (2012), these saturation curves are restricted to temperatures below that temperature, $T_{K,sat}$, at which $e_{v,\,sat} = P_{atmos}$. For the present case $T_{K,sat} = 370.44\,K$ was determined from the saturation temperature equation or "the Backward Equation", Eq. (31) of IAPWS (2007). For $T_K \geq T_{K,sat}$ the saturation quantities $e_{v,\,sat}$ and $de_{v,\,sat}/dT$ remain fixed at their values $T_{K,sat}$, but $\rho_{v,\,sat}$ is allowed to decrease with increasing temperatures, i.e., $\rho_{v,\,sat} = \rho_{v,\,sat}(T_{K,sat})[T_{K,sat}/T_K][P_{atmos}/P_{ST}]$, in accordance with Table 13.2 (page 497) of Wagner and Pruess (2002), where $P_{ST} = 101\,325\,Pa$ is the standard pressure. The present treatment of $\rho_{v,\,sat}$ is different from Massman (2012), who assumed that $\rho_{v,\,sat}(T_K \geq T_{K,sat}) = \rho_{v,\,sat}(T_{K,sat})$.

2.2.2 Functions related to water vapor: D_{ve}, u_{vl}, S_v

D_{ve} is modeled as:

$$D_{ve} = \tau(\eta - \theta)S_F\mathcal{E}D_v$$

where τ [$m\,m^{-1}$] is the tortuosity of soil with $\tau = 0.66[(\eta - \theta)/\eta]^3$ after Moldrup et al. (1997), $\mathcal{E}$ (*dimensionless*) is the vapor flow enhancement factor and is discussed in Massman (2012), D_v [$m^2\,s^{-1}$] is the molecular diffusivity of water vapor into the soil atmosphere, which will be taken as a mixture of both dry air and (potentially large

GMDD
8, 2555–2603, 2015

amounts of) water vapor, and $S_F = 1 + e_v/P_{atmos}$ (*dimensionless*) is Stefan correction or mass flow factor, which here is a linear approximation for the correct (mathematically hyperbolic) expression for S_F used in Massman's (2012) model and many other models of soil evaporation and vapor diffusion. The correct form for S_F is $S_F = 1/(1 - e_v/P_{atmos})$, which Massman (2012) and Campbell et al. (1995) further limit to a maximum value of 10/3 to avoid dividing by 0 as $e_v \to P_{atmos}$. The present linear formulation of S_F is relatively slower to enhance the vapor transport by diffusion than the hyperbolic form, but this is only of any real significance when $S_F \geq 1$. On the other hand because the linear form is not limited to any preset maximum value it compensates for these underestimations when $S_F > 10/3$.

D_v is estimated from the diffusivity of water vapor in dry air, $D_{vd} = D_{vd}(T_K)$ [$m^2\,s^{-1}$] and the self-diffusivity of water vapor in water vapor, $D_{vv} = D_{vv}(T_K)$ [$m^2\,s^{-1}$], where

$$D_{vd} = D_{vdST}\left(\frac{P_{ST}}{P_{atmos}}\right)\left(\frac{T_K}{T_{ST}}\right)^{\alpha_{vd}}$$

and

$$D_{vv} = D_{vvST}\left(\frac{P_{ST}}{P_{atmos}}\right)\left(\frac{T_K}{T_{ST}}\right)^{\alpha_{vv}}$$

and $T_{ST} = 273.15\,K$ is the standard temperature, $D_{vdST} = 2.12 \times 10^{-5}\,m^2\,s^{-1}$, $\alpha_{vd} = 7/4$, $D_{vvST} = 1.39 \times 10^{-5}\,m^2\,s^{-1}$, and $\alpha_{vv} = 9/4$. The parameters D_{vvST} and α_{vv} relate to the self-diffusion of water vapor and their numerical values were determined from a synthesis of results from Hellmann et al. (2009) and Yoshida et al. (2006, 2007). The uncertainty associated with this value for D_{vvST} is at least ±15 % and possibly more, e.g., Miles et al. (2012). Blanc's Law (Marrero and Mason, 1972) combines D_{vd} and D_{vv} to yield the following expressions for $D_v = D_v(T_K, \rho_v)$:

$$\frac{1}{D_v(T_K,\rho_v)} = \frac{1-\chi_v}{D_{vd}} + \frac{\chi_v}{D_{vv}} \quad \text{or} \quad D_v(T_K,\rho_v) = \frac{D_{vd}D_{vv}}{(1-\chi_v)D_{vv} + \chi_v D_{vd}}$$

GMDD
8, 2555–2603, 2015

The present model for the advective velocity associated with the volatilization of water, u_{vl}, is taken from Ki et al. (2005) and is non-equilibrium equivalent to that used by Massman (2012) in his equilibrium model. Here

$$\frac{\partial u_{vl}}{\partial z} = \frac{S_v}{(\eta - \theta)\rho_v} \tag{9}$$

where the basic assumptions are that both liquid water and vapor are Newtonian fluids and that only incompressible effects are being modeled. In essence Eq. (9) assumes that the vaporization of soil moisture acts as a steady-state (and rapidly expanding or "exploding") volume source term, which yields a 1-D advective velocity associated with volatilization of liquid water. For an equilibrium model of soil moisture evaporation that does not include water movement (i.e., $\mathcal{K}_H \equiv 0$, $\mathcal{K}_n \equiv 0$, and $V_{\theta,surf} \equiv 0$), then $S_v \equiv -\rho_w \partial\theta/\partial t$ (from Eq. 2 above), which demonstrates the connection between present model of u_{vl} with that used by Massman's (2012). But unlike Massman (2012), the present model does not require any numerical adjustments to Eq. (9) in order to maintain numerical stability.

The functional parameterization of S_v follows from the non-equilibrium assumption, i.e., $S_v \propto (\rho_{ve} - \rho_v)$, where $\rho_{ve} = a_w \rho_{v,\,sat}(T_K)$ [kg m^{-3}] is the equilibrium vapor density and $a_w = e^{\frac{M_w \psi_*}{RT_K}\psi_n}$ (*dimensionless*) is the water activity, modeled here with the Kelvin Equation. The difficult part is how to construct the proportionality coefficient. Nevertheless, there are at least a two ways to go about this: (a) largely empirically (e.g., Smits et al., 2011 and related approaches referenced therein), or (b) assume that $S_v = A_{wa} J_v$ (e.g., Skopp, 1985 or Novak, 2012), where A_{wa} [m^{-1}] is the volume-normalized soil water-air interfacial surface area and J_v [kg m^{-2} s^{-1}] is the flux to/from that interfacial surface. This second approach allows a more physically-based parameterization of the flux, viz., $J_v = \mathcal{R}_v(\rho_{ve} - \rho_v)$, where $\mathcal{R}_v$ [ms^{-1}] is the interfacial surface transfer coefficient. For example, Novak (2012) proposed that the flux be driven be diffusion, so that $\mathcal{R}_v = D_v/r_{ep}$, where r_{ep} [m] is the equivalent pore radius and D_v is the diffusivity of water vapor in soil air. After a bit of algebra and some simple geometrically-based

GMDD
8, 2555–2603, 2015

assumptions concerning the relationships between r_{ep}, a spherical pore volume, and A_{wa}, one arrives at ("the Novak") model of the source term:

$$S_v^{(N)} = S_*^{(N)} A_{wa}^2 D_v(\rho_{ve} - \rho_v)$$

where $S_*^{(N)}$ (*dimensionless*) is an adjustable model parameter.

But there is another way to model the vapor flux, J_v, which is also used in the present study. This second approach is based on the Hertz–Knudsen Equation, which has its origins in the kinetic theory of gases and describes the net flux of a gas that is simultaneously condensing on and evaporating from a surface. A general expression for the Hertz–Knudsen flux is $J_v = \sqrt{RT_K/M_w}(\mathcal{K}_e\rho_{ve} - \mathcal{K}_c\rho_v)$, where $\mathcal{K}_e$ (*dimensionless*) is the mass accommodation (or evaporation) coefficient and $\mathcal{K}_c = \mathcal{K}_c(T_K, \psi_n)$ (*dimensionless*) is the thermal accommodation (or condensation) coefficient. For the present purposes $\mathcal{K}_e \equiv 1$ can be assumed. This model of J_v yields the following model for S_v:

$$S_v^{(M)} = S_*^{(M)} A_{wa} \sqrt{\frac{RT_K}{M_w}}(\rho_{ve} - \mathcal{K}_c\rho_v) \tag{10}$$

where $S_*^{(M)}$ (*dimensionless*) is an adjustable model parameter, to be determined by "tuning" it as necessary to ensure model stability. This model for $S_v^{(M)}$ is now more or less complete, but the model for $S_v^{(N)}$ is neither quite complete nor precisely comparable to $S_v^{(M)}$. This is now remedied by introducing $\mathcal{K}_c$ into $S_v^{(N)}$ and subsuming a factor of A_{wa} into $S_*^{(N)}$, yielding:

$$S_v^{(N)} = S_*^{(N)} A_{wa} D_v(\rho_{ve} - \mathcal{K}_c\rho_v) \tag{11}$$

where $S_*^{(N)}$ [m^{-1}] now has physical dimensions, but otherwise remains an adjustable parameter that will be scaled such that $S_v^{(N)} \approx O(S_v^{(M)})$. In this form these two models

GMDD
8, 2555–2603, 2015

for S_v can be used to test the sensitivity of the model's solution to different temperature forcing, because $S_v^{(M)} \propto \sqrt{T_K}$, whereas $S_v^{(N)} \propto T_K^{\alpha}$, where $\alpha \geq 2$.

Concluding the development of S_v requires models of $\mathcal{K}_c$ and $A_{wa} = A_{wa}(\theta)$. $\mathcal{K}_c$ is parameterized as

$$\mathcal{K}_c(T_K, \psi_n) = e^{\frac{E_{av} - M_w \psi}{R}\left(\frac{1}{T_K} - \frac{1}{T_{K,in}}\right)}$$

where $T_{K,in}$ [K] is the initial temperature of the laboratory experiments and because $T_K \geq T_{K,in}$ throughout the experiment $\mathcal{K}_c \leq 1$ throughout the experiment and $E_{av} - M_w \psi$ [J mol^{-1}] is an empirically determined surface condensation/evaporation activation energy. Note: the enthalpy of vaporization, $h_v(T_K)$, is a logical choice for E_{av}. Nevertheless, model performance was significantly enhanced by simply assigning a constant value for $E_{av} \approx 30$ kJ mol^{-1} rather than using h_v. Mathematically this present formulation of $\mathcal{K}_c$ largely eliminates model instabilities by suppressing condensation relative to evaporation throughout the experiment and will be discussed in greater detail in a later section.

A_{wa} is parameterized as a parabolic function to simulate the conceptual model of A_{wa} proposed by Constanza-Robinson and Brusseau (2002: see their Fig. 1b):

$$A_{wa}(\theta) = \mathcal{S}_w(1 - \mathcal{S}_w)^{a_1} + a_2[\mathcal{S}_w(1 - \mathcal{S}_w)]^{a_3}$$

where $\mathcal{S}_w = \theta/\eta$ is the soil water saturation and $a_1 = 40$, $a_2 = 0.003$, and $a_3 = 1/8$. This particular functional form ensures that $A_{wa} = 0$ when the soil is completely dry, $\theta = 0$, and when fully saturated, $\mathcal{S}_w = 1$. This particular parameter value for a_1 was chosen so that the maximum value of A_{wa} occurs at $\mathcal{S}_w = 0.025$ $(= 1/a_1)$ in accordance with the model of Constanza-Robinson and Brusseau (2002).

2.2.3 Thermal transport properties: C_s, λ_s

The model for $C_s(T, \theta)$ is taken from Massman (2012): $C_s(\theta, T) = c_s(T)\rho_b + C_w(T)\theta$, where ρ_b [kg m^{-3}] is the soil bulk density; $c_s(T) = c_{s0} + c_{s1}T$ [J kg^{-1} K^{-1}] is the specific

GMDD
8, 2555–2603, 2015

heat capacity of soil; and $C_w(T) = C_{w0} + C_{w1}T + C_{w2}T^2$ [J m^{-3} K^{-1}] is the volumetric heat capacity of water; and the parameterization constants $c_{s0}, c_{s1}, C_{w0}, C_{w1}, C_{w2}$ are given by Massman (2012). Note that the present $C_s(\theta, T)$ results from approximating $C_w(T) \equiv c_{pw}(T)\rho_w(T_K)$ by $c_{pw}(T)\rho_w(T_{ST})$, where $c_{pw}(T)$ [J kg^{-1} K^{-1}] is the isobaric specific heat capacity of water, and $\rho_w(T_{ST}) = 1000\,\mathrm{kg\,m^{-3}}$. This substitution for $\rho_w(T_K)$ is only made for $C_w(T)$.

The present formulation for isobaric heat capacity of water, $c_{pw}(T)$, was developed from Yaws (1995) and confirmed by comparing to Wagner and Pruess (2002). In general $c_{pw}(T)$ is also a function of pressure (e.g., Wagner and Pruess, 2002), but this dependency can be ignored for the present purposes. Other parameterization of $c_{pw}(T)$ (i.e., Sato, 1990; Jovanović et al., 2009; Kozlowski, 2012) were also examined, but proved unsatisfactory. Finally, Kozlowski (2012) reports numerical values for the dry soil parameters c_{s0} and c_{s1} that are similar to those discussed in Massman (2012) and used with the present model.

The model of soil thermal conductivity, λ_s, is the sum of two terms. The first, $\lambda_s^{(1)}(\theta, T_K, \rho_v)$, is taken principally from Campbell et al. (1994) and the second, $\lambda_s^{(2)}(\theta, T_K)$, is taken from Bauer (1993). This second term incorporates the effects of high-temperature thermal (infrared) radiant energy transfer within the soil pore space, which may be significant for certain soils and high enough temperatures (e.g., Durany et al., 2010). $\lambda_s^{(1)}$ is summarized first and repeated here to emphasize the difference between the present model's functional parameterizations and those used in Massman (2012).

$\lambda_s^{(1)}$ is modeled as:

$$\lambda_s^{(1)}(\theta, T_K, \rho_v) = \frac{k_w\theta\lambda_w(T_K, \rho_w) + k_a[\eta - \theta]\lambda_a^*(\theta, T_K, \rho_v) + k_m[1 - \eta]\lambda_m}{k_w\theta + k_a[\eta - \theta] + k_m[1 - \eta]} \tag{12}$$

where $\lambda_a^*(\theta, T_K, \rho_v) = \lambda_a(T_K) + \lambda_v^*(\theta, T_K, \rho_v)$ is the apparent thermal conductivity of the soil air and is the sum of the thermal conductivity of moist soil air, λ_a, and λ_v^*, which

GMDD
8, 2555–2603, 2015

incorporates the effects of latent heat transfer; λ_m is the thermal conductivity of the mineral component of the soil, which is assumed to be independent of temperature and soil moisture; and k_w, k_a, and k_m (*dimensionless*) are generalized formulations of the de Vries weighting factors (de Vries, 1963). Campbell et al. (1994) formulate λ_v^* as proportional to the product of the enthalpy of vaporization (h_v), the vapor diffusivity (D_v), the Stefan factor (S_F), the slope of the saturation vapor pressure ($de_{v,\,sat}/dT$), and the parameter $f_w(\theta, T)$ (Campbell et al. (1995) also used in the diffusivity enhancement factor, $\mathcal{E}$). For present model λ_v^* is

$$\lambda_v^*(\theta, T_K, \rho_v) = \frac{\hat{\rho}_{ST} h_v f_w S_F D_v [de_{v,\,sat}/dT]}{P_{atmos}} \tag{13}$$

where $\hat{\rho}_{ST} = 44.65\,\mathrm{mol\,m^{-3}}$ is the molar density of the standard atmosphere. Equations (12) and (13) are the same as those used in Massman (2012), but numerically they yield quite results due to the different formulations for h_v, S_F, D_v, and $e_{v,\,sat} = e_{v,\,sat}(T_K)$. Otherwise the de Vries (1963) shape factors, the parameter f_w, and all related parameters are the same as in Massman (2012).

$\lambda_s^{(2)}$ is modeled as:

$$\lambda_s^{(2)}(\theta, T_K) = 3.8\sigma N^2 R_p T_K^3 \tag{14}$$

where $\sigma = 5.670 \times 10^8\,\mathrm{W\,m^{-2}\,K^{-4}}$ is the Boltzmann constant; $N = N(\theta) = 1 + \theta/(3\eta)$ is the medium's (*dimensionless*) index of refraction; R_p [m] is the soil's pore space volumetric radius; and the factor of 3.8 subsumes a numerical factor of 4, a (*dimensionless*) pore shape factor (= 1 for spherical particles), and the (*dimensionless*) emissivity of the medium ≈ 0.95 (by assumption). Furthermore $R_p = 10^{-3}$ m is assumed for all present model simulations, although it will be used in sensitivity analysis to assess model performance.

GMDD
8, 2555–2603, 2015

2.2.4 Water retention curve

In general a WRC is a functional relationship between soil moisture and soil moisture potential and temperature, i.e., $\theta = \theta(\psi, T)$, although the temperature dependency is often ignored and was of little consequence to Massman's (2012) model. The three WRCs tested in the present study have been adapted to include a residual soil moisture, $\theta_r = \theta_r(\psi, T)$ [$m^3\,m^{-3}$], which is an atypical parameterization for both θ_r and the soil moisture's temperature dependency. Under more normal soil environmental conditions θ_r is assumed to be bound so securely to soil mineral surfaces that it is normally taken as a fixed constant. For the present purposes the principal WRC is adapted from Massman (2012) and is

$$\theta(\psi_n, T_K) = -\frac{\theta_l}{\alpha_l}\ln(\psi_n) + \left[\theta_h - \theta_r(\psi_n, T_K)\right]\left[1 + (\alpha_h\psi_n)^4\right]^{-\frac{1}{p}} + \theta_r(\psi_n, T_K) \tag{15}$$

Where

$$\theta_r(\psi_n, T_K) = \theta_{r^*} e^{\frac{b_1 E_{av}(1-b_2\psi_n)}{R}\left(\frac{1}{T_K} - \frac{1}{T_{K,in}}\right)} \tag{16}$$

and θ_l [$m^3\,m^{-3}$] is the extrapolated value of the water content when $\psi = \psi_l = -1\,J\,kg^{-1}$; $\alpha_l = \ln(\psi_*/\psi_l) = 13.8155106$; and θ_h [$m^3\,m^{-3}$], α_h (*dimensionless*) and p (*dimensionless*) are parameters obtained from Campbell and Shiozawa (1992), θ_{r^*} [$m^3\,m^{-3}$] is a constant soil-specific parameter, such that $\theta_{r^*} \le 0.03$ is to be expected, and b_1 (*dimensionless*) and b_2 (*dimensionless*) are adjustable parameters, which are expected to satisfy $b_1 > 0$ and $0 \le b_2 < 1$. Note: further discussion concerning the original version of Eq. (15) can be found in Massman (2012).

There is a simple and physically intuitive argument for this particular parameterization of $\theta_r(\psi_n, T_K)$ in Eq. (16). First, under more normal soil environmental conditions, i.e., $T_K \approx T_{K,in}$ and at least $\psi_n < 1$ (if not $\psi_n \ll 1$), then it is reasonable to expect that $\theta_r \approx \theta_{r^*}$ and nearly constant throughout (what might be expected to be relatively small

GMDD
8, 2555–2603, 2015

variations in) those conditions. But as the temperature increases, it is also reasonable to assume that the increasing amounts of thermal energy will begin to overcome the forces holding the bound water to the soil mineral surfaces and that θ_r will decrease. Mathematically, then one might therefore expect that $\partial\theta_r/\partial T_K < 0$. Massman (2012: see his discussion of ψ_T) made similar arguments when he included the temperature dependency in his version of the same basic WRC. Consequently, the Eqs. (15) and (16) above offer a different approach to including temperature effects on the WRC that maintains the temperature dependent properties of WRCs outlined by Massman (2012). Second, as the temperature increases and the soil moisture (including θ_r) begins to decrease, the soil moisture potential ψ_n will begin to increase (or $\psi < 0$ will decrease in absolute terms while increasing in magnitude), which in turn (it is hypothesized) will tend to strengthen the forces holding the bound water. Therefore, one might expect that as the soil dries out $\partial\theta_r/\partial\psi_n > 0$, which will oppose, but not dominate the temperature effects, i.e., $b_2 < 1$. Equation (16) is designed to capture these two opposing influences, assuming of course that $T_K > T_{K,in}$. But, it is itself not intended to be a fully physically-based dynamical theory of the residual soil moisture. Such a theory is beyond the intent of the present study. The sole intent here is to test and evaluate whether a dynamical θ_r can improve the model's performance. And in so far as it may succeed at doing so, it will also indicate the value and need for a more detailed physically-based dynamical model of θ_r.

The present study also includes similar adaptations to two other WRCs so as to test the model's sensitivity to different WRCs. These WRCs, which will not be shown here, are taken from Groenevelt and Grant (2004) and Fredlund and Xing (1994).

2.2.5 Functions related to liquid water transport: $\mathcal{K}_n$, $\mathcal{K}_H$, $V_{\theta,surf}$

The hydraulic conductivities, $\mathcal{K}_n(\theta,T_K)$ and $\mathcal{K}_H(\theta,T_K)$, are given as follows:

$$\mathcal{K}_n = \frac{K_l K_R \rho_w}{\mu_w}\psi_* \quad \text{and} \quad \mathcal{K}_H = \frac{K_l K_R \rho_w}{\mu_w} g$$

GMDD
8, 2555–2603, 2015

where K_l [m^2] is the intrinsic permeability of the soil (a constant for any given soil), $K_R = K_R(\theta, \theta_r)$ (*dimensionless*) is the hydraulic conductivity function (HCF), which is an analytical expression that is often, but not exclusively, derived from the water retention curve (WRC), $g = 9.81\,m\,s^{-2}$ is the acceleration due to gravity. The model for intrinsic permeability, which is taken from Bear (1972), is $K_l = (6.17 \times 10^{-4}) d_g^2$; where d_g [m] is the mean or "effective" soil particle diameter. For the soils used in the present work (Campbell et al., 1995; Massman, 2012) d_g was estimated from Shiozawa and Campbell (1991) and Campbell and Shiozawa (1992) or simply assigned a reasonable value if no other information was available.

For present study five difference parameterizations for $K_R(\theta, \theta_r)$ were tested. Two were from Grant et al. (2010), i.e., their Eq. (18) (Burdine) and Eq. (19) (Mualem); the Van Genuchten and Nielson (1985) model, their Eq. (22) with the mathematical constraints imposed as suggested by Assouline and Or (2013); the Brooks and Corey (1964) model; and Eq. (18) of Assouline (2001). The reason for testing several models of the HCF is to determine how different formulations for the HCF might impact the model's performance when comparing to the laboratory observations. The following HCF is Assouline's (2001) model, which is a relatively simple formulation for the HCF and serves as the reference HCF for the model simulations.

$$K_R(\theta, \theta_r) = \left(1 - \left[1 - \left(\frac{\theta - \theta_r(\psi_n, T_K)}{\eta}\right)^{\frac{1}{m}}\right]^m\right)^n \tag{17}$$

where for the present application $0 < m < 1$, and $n > 1$.

The term $\rho_w V_{\theta,surf}$ in Eq. (2) represents the soil moisture movement caused by water molecules "hopping" or "skipping" along the surface of the water films due to a temperature gradient (e.g., Medved and Černý, 2011). The present model for $V_{\theta,surf}$ is adapted from the model of Gawin et al. (1999) and is given as:

$$V_{\theta,surf} = -D_{\theta s}\frac{\partial \theta}{\partial z} = -D_{\theta s}D_{\theta\psi}\frac{\partial \psi_n}{\partial z} - D_{\theta s}D_{\theta T}\frac{\partial T}{\partial z} \tag{18}$$

GMDD
8, 2555–2603, 2015

where $D_{\theta s} = D_{\theta s}(T_K, \theta)$ [$m^2\,s^{-1}$] is the surface diffusivity and is parameterized as:

$$D_{\theta s} = D_{\theta s0} \exp\left[-2\left(\frac{\theta}{\theta_b}\right)^{\beta}\left(\frac{T_{ST}}{T_K}\right)\right]$$

with $D_{\theta s0} \approx 10^{-7}\,m^2\,s^{-1}$, but is also adjusted as needed to maintain model stability and the quality of the model simulations; $\theta_b \approx 0.02$; and $\beta = 1/4$ when $\theta \geq \theta_b$ or otherwise $\beta = 1$ when $\theta < \theta_b$. Note this value for $D_{\theta s0}$ is often greater than that employed by Gawin et al. (1999), who suggested $D_{\theta s0} \approx 10^{-10}\,m^2\,s^{-1}$. $D_{\theta s0}$ is also discussed in more detail in the results section.

By expressing $V_{\theta,surf}$ in terms of the gradient of the "normalized" soil moisture potential, ψ_n, in Eq. (18), $\mathcal{K}_n^*$ and $\mathcal{K}_m$, used in Eqs. (5) and (6), can be identified as: $\mathcal{K}_n^* = \mathcal{K}_n + D_{\theta s} D_{\theta\psi}$ and $\mathcal{K}_m = D_{\theta s} D_{\theta T}$.

3 Numerical implementation

The numerical model as outlined above and detailed in this section is coded as MATLAB (The MathWorks Inc., Natick, MA, Version R2013b) script files.

3.1 Crank–Nicolson method

The linearized Crank–Nicolson method is used to solve Eqs. (5), (6), and (7). For Eq. (5) this yields the following (canonical) linear finite difference equation:

$$-A^j_{TTi}T^{j+1}_{i-1} + \left[1 + B^j_{TTi}\right]T^{j+1}_i - C^j_{TTi}T^{j+1}_{i+1} + A^j_{T\psi i}\psi^{j+1}_{ni-1} - \left[\Gamma^j_{T\psi i} - B^j_{T\psi i}\right]\psi^{j+1}_{ni} + C^j_{T\psi i}\psi^{j+1}_{ni+1}$$
$$= A^j_{TTi}T^j_{i-1} + \left[1 - B^j_{TTi}\right]T^j_i + C^j_{TTi}T^j_{i+1} - A^j_{T\psi i}\psi^j_{ni-1} - \left[\Gamma^j_{T\psi i} + B^j_{T\psi i}\right]\psi^j_{ni} - C^j_{T\psi i}\psi^j_{ni+1} \quad (19)$$

where j and $j+1$ are consecutive time indices, $i-1$, i, and $i+1$ are contiguous spatial indices, and $A^j_{TTi}, B^j_{TTi}, C^j_{TTi}, A^j_{T\psi i}, B^j_{T\psi i}$, $C^j_{T\psi i}$, and $\Gamma^j_{T\psi i}$ are the linearized C-N coefficients, which will not be explicitly listed here, but they do largely follow conventions and

GMDD
8, 2555–2603, 2015

notation similar to Massman (2012). Although containing more terms than Eq. (19), the finite difference equation corresponding to Eq. (6) is very similar. But to linearize Eq. (7), the Crank–Nicolson scheme requires linearizing the source term, $S_v(T,\theta,\psi,\rho_v)$. This is done with a first order Taylor series expansion of the C-N term S_v^{j+1} as follows:

$$S_{vi}^{j+1} = S_{vi}^{j} + \left(\frac{\delta S_v}{\delta T}\right)_i^j (T_i^{j+1} - T_i^j) + \left(\frac{\delta S_v}{\delta \psi_n}\right)_i^j (\psi_{ni}^{j+1} - \psi_{ni}^j) + \left(\frac{\partial S_v}{\partial \rho_v}\right)_i^j (\rho_{vi}^{j+1} - \rho_{vi}^j)$$

where $\frac{\delta S_v}{\delta T} = D_{\theta T}\frac{\partial S_v}{\partial \theta} + \frac{\partial S_v}{\partial T}$ and $\frac{\delta S_v}{\delta \psi_n} = D_{\theta\psi}\frac{\partial S_v}{\partial \theta} + \frac{\partial S_v}{\partial \psi_n}$, which in turn yields the following linearized finite difference equation for Eq. (7):

$$\begin{aligned}
&-\left[\frac{\Delta t}{2(\eta-\theta)_i^j}\left(\frac{\delta S_v}{\delta T}\right)_i^j\right] T_i^{j+1} - \left[B_{\rho\psi i}^j + \frac{\Delta t}{2(\eta-\theta)_i^j}\left(\frac{\delta S_v}{\delta \psi_n}\right)_i^j\right] \psi_{ni}^{j+1} \\
&- A_{\rho\rho i}^j \rho_{vi-1}^{j+1} + \left[1 + B_{\rho\rho i}^j - \frac{\Delta t}{2(\eta-\theta)_i^j}\left(\frac{\partial S_v}{\partial \rho_v}\right)_i^j\right] \rho_{vi}^{j+1} - C_{\rho\rho i}^j \rho_{vi+1}^{j+1} = \\
&-\left[\frac{\Delta t}{2(\eta-\theta)_i^j}\left(\frac{\delta S_v}{\delta T}\right)_i^j\right] T_i^{j} - \left[B_{\rho\psi i}^j + \frac{\Delta t}{2(\eta-\theta)_i^j}\left(\frac{\delta S_v}{\delta \psi_n}\right)_i^j\right] \psi_{ni}^{j} + A_{\rho\rho i}^j \rho_{vi-1}^{j} \\
&+\left[1 - B_{\rho\rho i}^j - \frac{\Delta t}{2(\eta-\theta)_i^j}\left(\frac{\partial S_v}{\partial \rho_v}\right)_i^j\right] \rho_{vi}^{j} + C_{\rho\rho i}^j \rho_{vi+1}^{j} + \frac{\Delta t}{(\eta-\theta)_i^j} S_{vi}^j
\end{aligned} \tag{20}$$

where $B_{\rho\psi i}^j$, $A_{\rho\rho i}^j$, $B_{\rho\rho i}^j$, and $C_{\rho\rho i}^j$ are linearized C-N coefficients related to the transport terms of Eq. (7) and Δt [s] is the time step. Here $\Delta t = 1.2$ s and was chosen after testing the model at $\Delta t = 0.3$ s and $\Delta t = 0.6$ s to ensure no degradation in model performance or solution stability at the larger time step.

GMDD
8, 2555–2603, 2015

3.2 Upper boundary conditions

The upper boundary condition on heat and vapor transfer are formulated in terms of the surface energy balance and, except for the latent heat flux, is identical to Massman's (2012) upper boundary condition.

$$\epsilon(\theta_0)Q_R^{\Downarrow}(t) = \epsilon(\theta_0)\sigma T_{K0}^4 + \rho_a\, c_{pa} C_H[T_0 - T_{amb}(t)] + L_{v0}E_0 + G_0 \tag{21}$$

where the "0" subscript refers to the surface and the terms from left to right are: the incoming or down welling radiant energy, $Q_R^{\Downarrow}(t)$ [$\mathrm{W\,m^{-2}}$], absorbed by the surface, which is partitioned into the four terms (fluxes) on the right side of the equation, the infrared radiation lost by the surface, the surface sensible or convective heat, the surface latent heat, and the surface soil heat flux. $Q_R^{\Downarrow}(t)$ and $T_{amb}(t)$ are functions of time and are prescribed externally as discussed in Massman (2012). The soil surface emissivity, $\epsilon(\theta_0)$ (*dimensionless*), is a function of soil moisture and is taken from Massman (2012), as is surface heat transfer coefficient C_H [$\mathrm{m\,s^{-1}}$]; and $\sigma = 5.670 \times 10^8\,\mathrm{W\,m^{-2}\,K^{-4}}$ is the Stefan–Boltzmann constant.

The surface evaporation rate, E_0 [$\mathrm{kg\,m^{-2}\,s^{-1}}$], is parameterized as

$$E_0 = h_{s0}\, C_E[\rho_{v0} - \rho_{v\,amb}(t)] \tag{22}$$

where $h_{s0} \equiv a_{w0} = \exp([M_w\psi_*\psi_{n0}]/[RT_{K0}])$ (*dimensionless*) is the "surface humidity", here modeled as the water activity at the surface using the Kelvin Equation; C_E [$\mathrm{m\,s^{-1}}$] is the surface the transfer coefficient, an adjustable model parameter but one that can reasonably be assumed to be between about $10^{-4}\,\mathrm{m\,s^{-1}}$ (Jacobs and Verhoef, 1997) and $10^{-3}\,\mathrm{m\,s^{-1}}$ (Massman, 2012). Finally, in the case of the laboratory experiments of Campbell et al. (1995), $\rho_{v\,amb}(t)$, like $T_{amb}(t)$ and $Q_R^{\Downarrow}(t)$, is an external forcing function at the soil surface. The present formulation of E_0 results from combining and adapting the expressions for the potential evaporation rate for soils developed by Jacobs and Verhoef (1997) and Eq. (9.14) of Campbell (1985). For this formulation the surface relative

GMDD
8, 2555–2603, 2015

humidity, h_{s0}, is the surface property that constrains or reduces the surface evaporation E_0 to less than the potential rate.

The upper boundary condition on soil water is $(\partial\theta/\partial z)_0 = 0$, which when employed with the WRC, Eq. (15), yields the following upper boundary condition on the conservation of soil moisture, Eq. (6):

$$\left(\frac{\partial \psi_n}{\partial z}\right)_0 = \left(\frac{D_{\theta T}}{D_{\theta \psi}}\right)_0 \frac{G_0}{\lambda_{s0}} \tag{23}$$

The boundary forcing functions $e_{v\,amb}(t)$ [Pa] (the ambient vapor pressure), $T_{amb}(t)$, and $Q_R^{\Downarrow}(t)$ are taken from Massman (2012), which in turn were adapted to the laboratory data of Campbell et al. (1995). They take the following generic form:

$$V(t) = V_i e^{-t/\tau} + V_f(1 - e^{-t/\tau})$$

where V_i is the value of the function at the beginning of the soil heating experiment, V_f is the value of the function at the end of the experiment, and τ [s] is a time constant of the heating source, which varies with each individual soil heating experiment. $\rho_{v\,amb}(t)$ is obtained from $e_{v\,amb}(t)$ and $T_{amb}(t)$ using the ideal gas law.

3.3 Lower boundary conditions and initial conditions

As with the companion model (Massman, 2012), a numerical (or extrapolative or "pass-through") lower boundary condition (Thomas, 1995) is also used for the present model. Analytically this is equivalent to assuming that the second spatial derivative $(\partial^2/\partial z^2)$ of all model variables is zero at the lower boundary. It is used here for the same reason as with the previous model: principally for convenience because it is likely to be nearly impossible to specify any other the lower boundary condition during a real fire. The boundary condition on the advective velocity is $u_{vl} = 0$ at the bottom boundary, which is also the same as with Massman (2012) and Campbell et al. (1995). Further discussion on the model's lower boundary conditions can be found in Massman (2012).

GMDD
8, 2555–2603, 2015

Except for the initial value of ψ_{in} (or $\psi_{n,in}$), all initial conditions (soil temperature and moisture content), which are assumed to be uniform throughout the soil column for each soil type and heating experiment, are taken directly from Campbell et al. (1995). The initial value for ψ is obtained by inverting (solving for it using) the WRC after inputing the initial values for soil temperature and moisture content. Consequently, $\psi_{n,in}$ can vary with the specific WRC.

4 Results

4.1 Recalibration of observed volumetric soil moisture

In the original soil heating experiments of Campbell et al. (1995) soil temperatures were measured with copper-constantan thermocouples at the sample surface and at 5, 15, 25, 35, 65, and 95 mm depth and changes in soil moisture were obtained by gamma ray attenuation at the same depths (except the surface). The moisture detecting system was linearly calibrated for each experimental run between (a) the initial soil moisture amounts, which were determined gravimetrically beforehand, and (b) the point at which the sample was oven-dried (also determined before the heating experiment) where $\theta = 0$ is assumed. But oven-drying a soil will not necessarily remove all the liquid water from a soil, i.e., a soil can display residual water content, θ_r, after oven-drying. Consequently, the soil moisture data obtained and reported by Campbell et al. (1995) show negative soil moistures at the time the soil dryness passes outside the oven-dry range. Massman (2012) commented on this issue. With the present study, all volumetric soil moisture data were first adjusted (using a linear transformation) to rescale the observed soil moisture, $\theta_{observed}$, so that the values of $\theta_{observed} < 0$ became $\theta_{observed} \approx 0$. This re-scaling had very little impact on any values of $\theta_{observed}$ except those asymptotic data where $\theta_{observed} < 0$. Furthermore, this re-calibration is reasonable so long as the original calibration was linear and based on a Beer's Law type extinction coeffi-

GMDD
8, 2555–2603, 2015

cient (which would be linearly related to the logarithm of the attenuation of gamma ray intensity).

4.2 Model performance

Like Massman (2012) the present study focuses on the results for one soil type: Quincy Sand with an initial volumetric soil moisture content of 0.14 $m^3\,m^{-3}$. This simplifies (and enhances the value of) the comparisons between the present non-equilibrium model with the equilibrium model of Massman (2012).

Figure 1 compares the measured (symbols) and modeled (lines) of soil temperature during the Quincy Sand heating experiment. The colors indicate the depths (mm) of the experimental and model data. (Note: the same color is also used to denote to same depth for both the model and observed data in Figs. 2–4.) The solid lines are model simulations that include the dynamic residual soil moisture, $\theta_r(\psi_n, T_K)$; the dashed lines correspond to simulations that exclude θ_r. The corresponding measured and modeled soil moisture is shown in Fig. 2. These two figures indicate that the present model produces results that are similar to both the original Campbell et al. (1995) model and the observations. Figure 2 suggests that the present model fairly faithfully captures the observed dynamic of moisture evaporating at higher levels and recondensing deeper in the soil where the temperatures are lower. Specifically, it seems to capture the observed amplitude of the recondensing moisture, but apparently not the corresponding total amount (greater duration or width of the recondensate). Including θ_r in the model also changes the soil moisture evaporative dynamic as well (Fig. 2). As was intended including a dynamic θ_r allows the model to capture the general shape (rate of decline) of the evaporating soil moisture curve, which is more or less impossible for the model without θ_r. But as Fig. 1 shows, the price for an improved simulation for the moisture dynamic is a somewhat poorer simulation of the temperature dynamic. Specifically this results from the longer evaporative period associated with the lower rates of evaporation, which in turn causes a longer delay time in the temperature rise. Nonetheless, comparing these two Figures with their counterparts in Massman (2012) clearly in-

GMDD
8, 2555–2603, 2015

dicates that the non-equilibrium model is a substantial improvement over the (older) equilibrium model, regardless of whether θ_r is included or not: a conclusion that is easily confirmed by comparing Figs. 4–7 below with their equivalents in Massman (2012).

Figure 3 is a plot of the data trajectory (observed soil temperatures vs. observed soil moistures for all the monitored depths). The model's solution trajectories (for the same depths, also with and without θ_r) are shown in Fig. 4. Comparing these two figures suggest that the model does a reasonable job of capturing the rapid vaporization of soil water at temperatures between 70 and 90 °C (at least at the depths below about 10 mm). And, as pointed in the previous two figures, the model also does a credible job of predicting the amplitude of the recondensing moisture ahead of the drying, but is less precise about the duration or width of the recondensation. Comparing the model results with and without the dynamic θ_r further indicates that the model with θ_r does a better job of capturing the "long evaporative tail" of the soil moisture. But when compared with observations (Fig. 3) the model with θ_r does not fully capture the amount of unevaporated soil moisture that remains at temperatures ≥ 150 °C. But this cannot be interpreted as a failure of the concept of a θ_r. Rather, θ_r is simply a "systems level" parameterization of the soil moisture bound to the soil mineral surfaces (presumably something akin to a molecular monolayer), it is not a detailed physically-based model of the evaporative energetics of surface-bound water. (Note: the parameter that controls the limiting value of θ_r is θ_{r^*} (see Eq. 16), which is set at 0.03, the maximum value at which it can be set. Attempting to capture more of the observed evaporative tail by adjusting θ_{r^*} upward can cause the model to become unstable.)

Figure 5 compares the vertical profiles of the soil temperatures at the end of the laboratory experiment with those at the end of the numerical simulation and Fig. 6 makes a similar comparison for the volumetric soil moisture content. These figures also include the modeling results synchronized in time and space with the observations, which are included to make the model output more directly comparable to the observations. (Note: the final vertical profiles obtained from the laboratory experiment are not coincident in time with the measurements made at any other depth. This is a consequence of the

GMDD
8, 2555–2603, 2015

experimental design, which required several minutes to complete one vertical scan for soil moisture.) The main emphasis here is on Fig. 6, because, as with the equilibrium model, the final temperature profile is largely determined by the moisture dynamics. The curves shown in this latter figure can be used to estimate the percentage amount of soil moisture evaporated and lost from the soil column at the end of the 90 min experiment. The laboratory observations suggests the 31 % was lost, the model (with θ_r) suggests 20 % was lost and the synchronized model suggests a 24 % loss. Not shown are the results for the model without θ_r which yielded a 25 % loss for the fully sampled model and a 27 % loss for the sub-sampled synchronized model. Because the fully sampled and sub-sampled model results give somewhat different percentage loss it is possible to conclude that the laboratory estimate of evaporative loss is likely biased (incorrect) because it is poorly resolved in time and space. So exact agreement between model and observations are in general unlikely. On the other hand, the present model results are significantly better than the equilibrium model, which found that no water was lost during the experiment, a clearly implausible result! (Rather than actually transporting the evaporated water out of the soil column, the equilibrium model "pushed" the moisture deeper into the soil ahead of the evaporative front.) Nonetheless and despite the fact that the present estimates of evaporative loss are clearly a major improvement over the equilibrium results, both model solutions produce a relatively sharply delineated advancing drying front, which is reminiscent of a Stefan-like or moving-boundary condition problem (e.g., see Whitaker and Chou 1983–1984 or Liu et al., 2005). So neither model actually captures the final moisture profile, nor fully captures the evaporative/moisture dynamic. Finally, the main difference between the model with and without θ_r is that without θ_r the model produces a deeper dry layer behind the drying front, mainly because without θ_r the model evaporates water more easily.

Figure 7 shows the final modeled profiles of soil vapor density, $\rho_v(z)$, equilibrium vapor density, $\rho_{ve}(z)$, and the condensation term, $\mathcal{K}_c(z)\rho_v(z)$, used with the non-equilibrium model source term, S_v (Eqs. 10 and 11), at the end of the 90 min model

GMDD
8, 2555–2603, 2015

simulation. The solid lines are model simulations that include the dynamic residual soil moisture, θ_r; the dashed red line corresponds to the simulation of $\rho_v(z)$ that does not include θ_r. The maximum soil vapor density occurs at about 40 mm where the evaporative source term is greatest, i.e., where $\rho_{ve}(z) - \mathcal{K}_c(z)\rho_v(z)$ is maximal, and where the moisture gradient is steepest, which is just ahead of the drying front (Fig. 6). Furthermore, the ρ_v profile suggests that there are both upward and downward diffusional fluxes of vapor away from the maximal evaporative source. The upward-directed flux escapes through the soil surface and into the ambient environment of the laboratory (the surface evaporative flux) and the downward-directed flux eventually recondenses below of the dry front. The equilibrium model, on the other hand, produced virtually no vapor gradient within the dry zone thereby contributing to the model' inability to allow any moisture to escape (evaporate) from the modeling domain. Unfortunately, there are no observations with which to check either models' predictions of vapor density, but at least intuitively, the present model's result seem reasonable and are certainly much more plausible than those of the equilibrium model.

If there is an implausibility with the present model it might be the soil vapor pressure, e_v, as shown in Fig. 8. Either with or without θ_r the non-equilibrium model suggests that e_v at the top of the soil column is between 3 and 4 standard atmospheres (300–400 kPa). This is a bit unexpected because pressure at the open end of the column might be expected (at least by this author) to be close to equilibrium with the ambient pressure (≈ 92 kPa). Although there are no data against which to check this result, there are other modeling results that lend some support to the present predictions for e_v. First, (Fig. 5 of) Udell's (1983) steady state model of a sand-water-steam system heated from above indicates that the environment within the modeling domain is likely to be super-saturated and that at a minimum e_v is greater than P_{atmos} by $\approx 5\,\%$ but (depending on the algorithmic treatment of the saturation vapor pressure and the exact value of P_{atmos} he used for his simulations) it is also plausible to expect that $e_v \approx (2 - -5)P_{ST}$. (Note that for Udell's (1983) simulations the maximum model temperature was about 180 °C and that he also modeled advective velocity using Darcy's law.) Second,

GMDD
8, 2555–2603, 2015

two different models of heated cement (Dayan, 1982 and Dal Pont et al., 2011) indicate that near the top surface of the model domain e_v can display values of $\approx$ (2–15) P_{ST}. The overall similarities between these three earlier models and the present non-equilibrium model make it impossible to completely invalidate the present model's predictions for e_v. Furthermore, the non-equilibrium model imposes no particular constraint on e_v – it is calculated using the ideal gas law and the profiles of vapor density and temperature, both of which appear plausible. Consequently, the somewhat surprising result shown in Fig. 8 appears to be a natural consequence of the physics underlying the basic model equations: the conservation of mass and thermal energy.

4.3 Sensitivity analysis

4.3.1 Source term, thermal conductivity, surface evaporation rate

There is little doubt that the present non-equilibrium model is an improvement over the equilibrium model of Massman (2012) and central to the success of the present model is the functional parameterization of the source term, S_v, and the related condensation coefficient, $\mathcal{K}_c(T_K, \psi_n)$. Basically $\mathcal{K}_c$ was required to maintain model stability especially at high temperatures; without it the model was unstable and the dynamic between moisture and vapor was non-physical. Regarding $\mathcal{K}_c$, the model is weakly sensitive to the choice of the surface evaporation/condensation activation energy, E_{av}, providing it does not vary much outside the range of $20\,\mathrm{kJ\,mol^{-1}} \le E_{av} \le 40\,\mathrm{kJ\,mol^{-1}}$. On the other hand, from a systems perspective it is very difficult to infer much about the details of the (high-temperature) physical processes associated with $\mathcal{K}_c$ or of the generality/universality of E_{av}, other than their apparent existence and utility to the present model. The best value for the scaling parameter, $S_*^{(M)}$, was within the range of about 0.5 to 1. The Novak model of the source term, $S_v^{(N)}$, also required the same $\mathcal{K}_c$, but the additional temperature dependency of $S_v^{(N)}$ over $S_v^{(M)}$ forced the soil moisture to evaporate at slightly lower temperatures (therefore sooner) than shown in Fig. 4 for

GMDD
8, 2555–2603, 2015

$S_v^{(M)}$. $S_v^{(N)}$ also eliminated an initial transient/instability that occurred with the $S_v^{(M)}$ solution (not shown here). Otherwise, the differences between $S_v^{(N)}$ and $S_v^{(M)}$ were not significant.

Recall that the soil thermal conductivity term $\lambda_s^{(2)}$ accounts for the effects of the high-temperature thermal infrared radiant energy transfer within the soil pore space and that the key parameter that controls $\lambda_s^{(2)}$ is R_p, the equivalent pore-volume radius. For values of R_p less than (and about equal to) the nominal value of 10^{-3} m used here R_p has very little influence on the model performance. But it is possible to improve the model's fidelity to the observed soil temperatures by increasing R_p to 6×10^{-3} m, at least for the Quincy sand data shown in Figs. 1 and 5. But the cost of this improvement are significantly higher values of soil vapor density (than shown in Fig. 7) and vapor pressure (than shown in Fig. 8). Consequently, in general $\lambda_s^{(2)}$ is only likely to be significant for highly porous soils, but on the other hand and in the present setting, improving one aspect of the model's performance may alter (or even degrade) other aspects.

The most important parameter controlling surface evaporation rate is the surface transfer coefficient C_E, to which the model is reasonably sensitive. In particular (and similar to Massman's 2012 results), the best (maximal) values of C_E were universally about $10^{-3}\,m\,s^{-1}$ and values much above this caused the model to become unstable. Values well below these values (and closer to the theoretical value of $10^{-4}\,m\,s^{-1}$) did not produce results much different than those resulting from $C_E = 10^{-3}\,m\,s^{-1}$. Nevertheless, C_E does play a weak role in determining the soil surface temperature and therefore can influence the magnitude of the surface convective heat flux.

4.3.2 Water retention curves and hydraulic conductivity functions

The two other WRCs tested for model performance were Groenevelt and Grant (2004) (GG04) and Fredlund and Xing (1994) (FY94). But prior to implementing them in the model they were both calibrated to be numerically similar near the dry end ($\theta \leq \approx 0.03$)

GMDD
8, 2555–2603, 2015

of Eq. (15). Their performance was initially tested with the Assouline HCF, Eq. (17) (henceforth abbreviated AS01), and then using other HCFs. In general, GG04+AS01 produced a slightly better simulation of the laboratory data than shown in the previous sections. Whereas, FY01+AS01 gave only non-physical results ending in a numerical instability. On the other hand pairing FY01 with the Burdine version of HCF from Grant et al. (2010) yielded a very good simulation of the laboratory soil moisture dynamics, at the expense of under-predicting the soil temperatures significantly; but pairing GG04 with the same HCF yielded a non-physical numerically unstable solution. Other combinations of WRCs and HCFs were also tested, but in general, all that can be concluded is that: (1) with the possible exception of GG04+AS01, the present pairing of WRC and HCF (Eq. 15 + AS01) gave the most consistent physically realistic performance and (2) where physically realistic simulations were produced (and therefore could be compared) the results were either similar to the present simulation (i.e., Eq. 15 + AS01) or yielded a very good simulation of one laboratory variable at the expense of another. Finally, no combination of WRCs or HCFs improved much on the present model simulation of the soil vapor density or the soil vapor pressure. Consequently, in the broadest terms if a stable model solution exists, it appears to be fairly robust relative to different WRCs and HCFs.

Although five different HCFs are tested here, there was one term that was universal to all of them: $V_{\theta,\mathrm{surf}}$ with its scaling parameter $D_{\theta\mathrm{s0}}$, which as explained above was incorporated into the normalized hydraulic function, $\mathcal{K}_\mathrm{n}^*$ (see Eq. 6 and the related discussion). The model was relatively insensitive to the exact value of $D_{\theta\mathrm{s0}}$ and $D_{\theta\mathrm{s0}} \approx 10^{-7}\,\mathrm{m^2\,s^{-1}}$ was almost universally the best choice for model performance (although the differences between model simulations with different values of $D_{\theta\mathrm{s0}}$ were rather small). Nonetheless, the more important question is: Of what significance are the transport mechanisms ($\mathcal{K}_\mathrm{n}$, $\mathcal{K}_\mathrm{H}$, and $V_{\theta,\mathrm{surf}}$) themselves to the model performance? This was evaluated by setting $K_\mathrm{l} = 0$ (thereby eliminating $\mathcal{K}_\mathrm{n}$ and $\mathcal{K}_\mathrm{H}$) and reducing $D_{\theta\mathrm{s0}}$ by 8–10 orders of magnitude (thereby reducing $V_{\theta,\mathrm{surf}}$ to insignificance) and then rerunning the model with each of the three different WRCs. For the Quincy Sand case,

GMDD
8, 2555–2603, 2015

both the present WRC, Eq. (15), and GG04 produced stable realistic solutions that did not differ much from those shown in the previous sections. And again GG04 was a slight improvement over Eq. (15). But, on the other hand, FY94 produced a physically unrealistic solution, which eventually ended in a model instability. It is also noteworthy that the other two stable WRCs yielded simulations of the modeled moisture dynamics that were degraded (compared to those with liquid moisture transport included), but somewhat better temperature dynamics. In summary, the present model (again when stable) appears to be less sensitive to differences in the HCFs than to the absence or presence of any HCF within the model.

On the other hand, there is a very good reason for including soil liquid moisture transport (a HCF) when applying this or similar models to a field setting, particularly those involving slash pile burns. As Massman (2012) points out, the rate of heating that occurs in the field may be 2–3 orders of magnitude less than that achieved in these laboratory studies. In addition, the heating in the field may extend 1–2 orders of magnitude longer than these 60–90 min experiments. Consequently, in a field setting, the scales associated with the length and intensity of a fire are much more amenable to soil moisture movement by soil hydraulics than is likely to be the case in the present laboratory setting.

4.3.3 Different soils with different initial conditions

The present model was used to simulate four other soil heating experiments besides the current Quincy Sand experiment, which had an initial soil moisture content = θ_{in} = $0.14\,m^3\,m^{-3}$. These others are (1) Dry Quincy Sand with $\theta_{in} = 0.03\,m^3\,m^{-3}$, (2) Dry Palousse B with $\theta_{in} = 0.07\,m^3\,m^{-3}$, (3) Moist Palousse B with $\theta_{in} = 0.17\,m^3\,m^{-3}$, and (4) Wet Boulder Creek with $\theta_{in} = 0.22\,m^3\,m^{-3}$. Only the two most extreme cases, Dry Quincy Sand and Wet Boulder Creek, offered any new insights. The other two cases just reinforced previous conclusions concerning model performance. In the case of Dry Quincy Sand, the model fit was improved by reducing the residual soil moisture

GMDD
8, 2555–2603, 2015

parameter, θ_{r^*}, to 0.005. This adjustment is contrary to the notion that θ_{r^*} is more or less constant for any given soil and is not expected to be influenced by the initial state of that soil. On the other hand, as mentioned earlier, the present formulation for θ_r is principally exploratory and heuristic, and not intended to be physically-based theory of the evaporative energetics of bound water. In the case of the Wet Boulder Creek soil, the model time step had to be reduced by half (to 0.6 s) in order to keep the model stable. Furthermore the solution was significantly degraded with the inclusion θ_r, again contrary to expectations. In general the present WRC, Eq. (15), without θ_r simulated the temperature and moisture dynamics (including the long evaporative tail) best. Summarizing all five experimental test cases, suggests that simulations of drier soils are better than those of wetter soils. In other words, when the soil is dry the temperature dynamics are usually well described by the model, but with increasing amounts of soil moisture the model's ability to simultaneously capture the dynamics of both soil moisture and temperature degrades. This suggests that the thermal energy dynamics are likely to be well described in the present model (which may well be true more generally of any soil heating model that employ variants of Eqs. (1) or (5)), but that the model's description of evaporative dynamics of soil moisture (and possibly soil moisture and soil vapor transport as well) is still incomplete.

4.3.4 The advective velocity, u_{vl}

Unlike with the companion model (Massman, 2012), the present model did not require reducing the magnitude of u_{vl} in order to maintain model stability, which again reinforces the impression that the present non-equilibrium model is an improvement over equilibrium model. Nonetheless, the present model can produce extraordinary gradients of vapor density and vapor pressure, which begs the question of whether such gradients could induce other types of mass transport than that captured by the present formulation of u_{vl}, Eq. (9). This was tested by using a model for Darcy's Law type formulation based on the assumption that the advective velocity is proportional to the vapor pressure gradient ($u_{vl} \propto -\partial e_v/\partial z$). This formulation was tested by incorporating it into

GMDD
8, 2555–2603, 2015

the model (excluding θ_r). But the model became unstable because mathematically the result is strongly hyperbolic, rather than predominantly parabolic. Further modeling development and parameterization of u_{vl} and vapor transport in general are well beyond the intent of the present study. But it is still possible to conclude that such exploration is warranted and could help improve model performance.

5 Summary and recommendations

This study has developed and tested a non-equilibrium model for simulating heat and moisture flow in soils during fires. By and large the simulations of soil temperature and moisture are credible. But simulated vapor density and pressure could exceed one or more standard atmospheres. Nonetheless, all model results showed a significant improvement over all comparable results from the companion equilibrium model of Massman (2012). The principal reason for the present model's success is the incorporation of a dynamic condensation coefficient, $\mathcal{K}_c$ (parameterized as a function of temperature and soil water potential), into the non-equilibrium evaporative source term, S_v; both of which are modeled after the Hertz–Knudsen Equation. Physically $\mathcal{K}_c$ suppressed condensation in favor of evaporation at high temperatures and soil water potentials, which in turn insured model stability. Furthermore, the non-equilibrium assumption also seemed to have improved the parameterization (and performance) of the mass transport associated with the advective velocity, u_{vl}, relative to the model's of Massman (2012) and Campbell et al. (1995). Another important (and novel) feature of the model is the inclusion of a dynamic residual soil moisture θ_r, also parameterized as a function of temperature and soil water potential, which is introduced into the model in an attempt to capture the long evaporative tail that seems to require temperatures well beyond 100 °C in order to evaporate at all. Physically θ_r is intended to represent the strongly bound soil moisture, which for the present purposes is conceptualized as a mono-layer.

GMDD
8, 2555–2603, 2015

Model performance is tested against laboratory measurements of soil temperature and moisture changes at several depths during controlled laboratory heating events (Campbell et al., 1995). Qualitatively, the model agrees with the laboratory observations, viz., it simulates an increase in soil moisture ahead of the drying front (due to the condensation of evaporated soil water at the front) and a hiatus in the soil temperature rise during the strongly evaporative stage of the soil drying. Furthermore, the model also captures the observed rapid evaporation of soil moisture that occurs at relatively low temperatures (50–90 °C), as well as some aspects of the long evaporative tail associated with strongly bound soil moisture. But, more often than not, the best simulations were usually a compromise between faithfully representing the observed soil temperatures or the observed soil moistures. The model also the displayed a tendency to predict a greater depth of the drying front than suggested by the observations. This over-prediction of the dry zone depth is also associated with the model's tendency to under-predict the duration of the long evaporative tail.

Sensitivity analyses (SAs) were also performed with different formulations for the water retention curve, soil hydraulic conductivity function, one variant of the present S_v, and different soil types with different initial conditions. In general, the SAs showed only slight or nuanced departures from the "standard" model solution shown in the Figs. 1–8. So the present model appears to be fairly robust and relatively insensitive to these aspects of the model. But it was also noted that as the initial soil moisture increased the model performance and the quality of the simulation would often degrade.

In conclusion, improving the present model requires both observational and theoretical investigations into the energetics, thermodynamics, and evaporative dynamics of water that is bound directly to the surfaces of soil particles. This in turn should provide better insights and improved parameterizations of S_v and θ_r. It should also prove insightful to test the present model's performance or the present formulations for S_v and θ_r against the more benign daily cycles of soil heating and associated moisture transport. And finally, improving the physical understanding and modeling of the advective flow velocity could also improve the present model's performance, because this

GMDD
8, 2555–2603, 2015

would likely improve the physical representation of the transport and redistribution of soil water vapor during fires.

Acknowledgements. All modeling code and data used in this paper are freely available from the author.

I would like to thank Gaylon S. Campbell for providing the laboratory data used in this study, as well as James W. Thomas for his insights into and discussions of the mathematical and numerical issues I encountered during the development of this model and Allan H. Harvey for his aid with the published resources used in parameterizing the self diffusion of water vapor.

References

Assouline, S.: A model for the relative hydraulic conductivity based on the water retention curve, Water Resour. Res., 37, 265–271, 2001.

Assouline, S. and Or, D.: Conceptual and parametric representation of hydraulic properties: a review, Vadose Zone J., 12, 1–20, doi:10.2136/vzj2013.07.0121, 2013.

Aston, A. R. and Gill, A. M.: Coupled soil moisture, heat and water vapour transfers under simulated fire conditions, Aust. J. Soil Res., 14, 55–66, 1976.

Bauer, T. H.: A general analytical approach toward the thermal; conductivity of porous media, Int. J. Heat Mass Tran., 36, 4181–4191, 1993.

Bear, J.: Dynamics of Fluids in Porous Media, American Elsevier Pub. Co, New York, NY, USA, 1972.

Bridge, L., Bradean, R., Ward, M. J., and Wetton, B. R.: The analysis of a two-phase zone with condensation in a porous medium, J. Eng. Math., 45, 247–268, 2003.

Brooks, R. H. and Corey, A. T.: Hydraulic Properties of Porous Media, Hydrology Paper 3, Colorado State University, Fort Collins, CO, USA, 1964.

Bücker, D., Span, R., and Wagner, W.: Thermodynamic property models for moist air and combustion gases, J. Eng. Gas Turb. Power, 125, 374–384, 2003.

Campbell, G. S.: Soil Physics with BASIC, Elsevier, New York, NY, USA, 1985.

Campbell, G. S. and Shiozawa, S.: Prediction of hydraulic properties of soils using particle-size distribution and bulk density data, in: Indirect Methods for Estimating the Hydraulic Properties of Unsaturated Soils, edited by: van Genuchten, M. T., University of California, Riverside, CA, 317–328, 1992.

GMDD

8, 2555–2603, 2015

Campbell, G. S., Jungbauer Jr., J. D., Bidlake, W. R., and Hungerford, R. D.: Predicting the effect of temperature on soil thermal conductivity, Soil Sci., 158, 307–313, 1994.
Campbell, G. S., Jungbauer Jr., J. D., Bristow, K. L., and Hungerford, R. D.: Soil temperature and water content beneath a surface fire, Soil Sci., 159, 363–374, 1995.
Constanza-Robinson, M. S. and Brusseau, M. L.: Air-water interfacial areas in unsaturated soils: evaluation of interfacial domains, Water Resour. Res., 38, 1195, doi:10.1029/2001WR000738, 2002.
Costa, V. A. F., Mendoça, M. L., and Figueiredo, A. R.: Modeling and simulation of wetted porous thermal barriers operating under high temperature or high heat flux, Int. J. Heat Mass Tran., 51, 3342–3354, 2008.
Dal Pont, S., Meftah, F., and Schrefler, B. A.: Modeling concrete under severe conditions as a multiphase material, Nucl. Eng. Des., 241, 562–572, 2011.
Danielewicz-Ferchmin, I. and Mickiewicz, A. R.: Water Density in the Double Layer, J. Phys. Chem., 100, 17281–17286, 1996.
Dayan, A.: Self-similar temperature, pressure and moisture distribution within an intensely heated porous half space, J. Heat Transf., 25, 1469–1476, 1982.
de Vries, D. A.: Simultaneous transfer of heat and moisture in porous media, EOS T. Am. Geophys. Un., 39, 909–916, 1958.
de Vries, D. A.: Thermal properties in soils, in: Physics of Plant Environment, edited by: van Wijk, W. R., North Holland Publishing Co., Amsterdam, 201–255, 1963.
di Blasi, C.: Simultaneous heat, mass, and momentum transfer during biomass drying, in: Developments in Thermochemical Biomass Conversion, edited by: Bridgwater, A. V. and Boocock, D. G. B., Springer Science + Business Media, Dordrecht, 117–131, 1997.
Durany, J., Fraga, B., and Vargas, F.: Physical modelling and numerical simulation of soil heating under forest fire conditions, in: Forest Fire Research, edited by: Viegas, D. X., ADAI/CEIF, Coimbra, Portugal, paper no. 263 of the attached CD, 2010.
Fredlund, D. G. and Xing, A: Equations for the soil-water characteristic curve, Can. Geotech. J., 31, 521–532, 1994.
Gawin, D., Majorana, C. E., and Schrefler, B. A.: Numerical analysis of hydro-thermal behavior and damage of concrete at high temperatures, Mech. Cohes.-Frict. Mat., 4, 37–74, 1999.
Grant, C. D., Groenevelt, P. H., and Robinson, N. I.: Application of the Grant–Groenevelt soil water retention model to predict the hydraulic conductivity, Aust. J. Soil Res., 48, 447–458, 2010.

GMDD
8, 2555–2603, 2015

Groenevelt, P. H. and Grant, C. D.: A new model for the soil-water retention curve that solves the problem of residual water contents, Eur. J. Soil Sci., 55, 479–485, 2004.
Gupta, H. V. and Nearing, G. S.: Debates – the future of hydrological sciences: a (common) path forward? Using models and data to learn: a systems theoretic perspective on the future of hydrological science, Water Resour. Res., 50, 5351–5359, doi:10.1002/2013WR015096, 2014.
Hellmann, R., Bich, E., Vogel, E., Dickinson, A. S., and Vesovic, V.: Calculation of the transport and relaxation properties of dilute water vapor, J. Chem. Phys., 131, 014303, doi:10.1063/1.3158830, 2009.
Huber, M. L., Perkins, R. A., Laeseche, A., Friend, D. G., Sengers, J. V., Assael, M. J., Metaxa, I. N., Vogel, E., Mareš, R., and Miyagawa, K.: New international formulation for the viscosity of H_2O, J. Phys. Chem. Ref. Data, 38, 101–125, 2009.
Huber, M. L., Perkins, R. A., Friend, D. G., Sengers, J. V., Assael, M. J., Metaxa, I. N., Miyagawa, K., Hellmann, R., and Vogel, E.: New international formulation for the thermal conductivity of H_2O, J. Phys. Chem. Ref. Data, 41, 033102, doi:10.1063/1.4738955, 2012.
IAPWS (The International Association for the Properties of Water and Steam): Revised Release on the IAPWS Industrial Formulation 1997 for the Thermodynamic Properties of Water and Steam, available at: http://www.iapws.org (last access: 24 May 2013), 2007.
Jacobs, A. F. and Verhoef, A.: Soil evaporation from sparse natural vegetation estimated from Sherwood numbers, J. Hydrol., 188–189, 443–452, 1997.
Jovanović, J. D., Knežević-Stevanović, A. B., and Grozdanić, D. K.: An empirical equation for temperature and pressure dependence of liquid heat capacity, J. Taiwan Inst. Chem. E., 40, 105–109, 2009.
Kadoya, K., Matsunaga, N., and Nagashima, A.: Viscosity and thermal conductivity of dry air in the gaseous phase, J. Phys. Chem. Ref. Data, 14, 947–970, 1985.
Kapoor, A., Yang, R. T., and Wong, C.: Surface diffusion, Catal. Rev., 31, 129–214, 1989.
Ki, H., Mohanty, P. S., and Mazumder, J.: A numerical method for multiphase incompressible thermal flows with solid–liquid and liquid–vapor phase transformations, Num. Heat Transf., Part B: Funds., 48, 125–145, 2005.
Kozlowski, T.: Modulated Differential Scanning Calorimetry (MDSC) studies on low-temperature freezing of water adsorbed on clays, apparent specific heat of soil water and specific heat of dry soil, Cold Reg. Sci. Technol., 78, 89–96, 2012.

GMDD
8, 2555–2603, 2015

Lynch, D. R.: Numerical Partial Differential Equations for Environmental Scientists and Engineers, Springer, New York, NY, 2005.
Marrero, T. R. and Mason, E. A.: Gaseous diffusion coefficients, J. Phys. Chem. Ref. Data, 1, 3–118, 1972.
Massman, W. J.: Modeling soil heating and moisture transport under extreme conditions: forest fires and slash pile burns, Water Resour. Res., 48, W10548, doi:10.1029/2011WR011710, 2012.
Medved, I. and Černý, R.: Surface diffusion in porous media: a critical review, Micropor. Mesopor. Mat., 142, 405–422, 2011.
Miles, R. E. H., Reid, J. P., and Rüpinen, I.: Comparison of approaches for measuring the mass accommodation coefficient for the condensation of water and sensitivities to uncertainties in thermophysical properties, J. Phys. Chem. A, 116, 10810–10825, 2012.
Milly, P. C. D.: Moisture and heat-transport in hysteretic, inhomogeneous porous media: a matric head-based formulation and a numerical model, Water Resour. Res., 18, 489–498, 1982.
Moldrup, P. T., Olesen, D. E., Roslton, D. E., and Yamaguchi, T.: Modeling diffusion and reactions in soils: VII. Predicting gas and ion diffusivity in undisturbed and sieved soils, Soil Sci., 162, 632–640, 1997.
Neary, D. G., Ryan, K. C., and DeBano, L. F. (Eds.): Wildland Fire in Ecosystems, General Technical Report RMRS-GTR-42-vol.4, USDA Forest Service, Ogden, UT, 2005.
Novak, M. D.; Dynamics of the near-surface evaporation zone and corresponding effects on the surface energy balance of a drying soil, Agr. Forest Meteorol., 150, 1358–1365, 2010.
Novak, M. D.: Comment on "Evaporation from soils under thermal boundary conditions: experimental and modeling investigation to compare equilibrium- and nonequilibrium-based approaches" by Kathleen M. Smits, Abdullah Cihan, Toshihiro Sakaki, and Tissa H. Illangasekare, Water Resour. Res., 48, W05549, doi:10.1029/2011WR011393, 2012.
Ouedraogo, F., Cherblanc, F., Naon, B., and Bénet, J.-C.: Water transfer in soil at low water content. Is the local equilibrium assumption still appropriate?, J. Hydrol., 492, 117–127, 2013.
Philip, J. R. and de Vries, D. A.: Moisture movement in porous materials under temperature gradients, EOS T. Am. Geophys. Un., 38, 222–232, 1957.
Sato, H.: An equation of state for the thermodynamic properties of water in the liquid phase including the metastable state, in: Properties of Water and Steam Proceedings of the 11th International Conference, edited by: Píchal, M. and Šifner, O., Hemisphere Publishing Company, New York, NY, USA, 48–55, 1990.

GMDD
8, 2555–2603, 2015

Shiozawa, S. and Campbell, G. S.: On the calculation of mean particle diameter and standard deviation from sand, silt, and clay fractions, Soil Sci., 152, 427–431, 1991.
Skopp, J.: Oxygen uptake and transport in soils: analysis of the air-water interfacial area, Soil Sci. Soc. Am. J., 49, 1327–1331, 1985.
Smits, K. M., Cihan, A., Soshihiro, T., and Illangasekare, T. H.: Evaporation from soils under thermal boundary conditions: experimental and modeling investigation to compare equilibrium- and nonequilibrium-based approaches, Water Resour. Res., 47, W05540, doi:10.1029/2010WR009533, 2011.
Smits, K. M., Cihan, A., Ngo, V. V., and Illangasekare, T. H.: Reply to comment by Michael D. Novak on "Evaporation from soils under thermal boundary conditions: experimental and modeling investigation to compare equilibrium- and nonequilibrium-based approaches", Water Resour. Res., 48, W05550, doi:10.1029/2011WR011609, 2012.
Somayajulu, G. R.: New equations for enthalpy of vaporization from the triple point to the critical point, Int. J. Thermophys., 9, 567–575, 1988.
Thomas, J. C.: Numerical Partial Differential Equations: Finite Difference Methods, Springer, New York, NY, USA, 1985.
Tsilingiris, P. T.: Thermophysical transport properties of humid air at temperature range between 0 and 100 °C, Energy Convers. Manage., 49, 1098–1110, 2008.
Udell, K. S.: Heat transfer in porous media heated from above with evaporation, condensation, and capillary effects, J. Heat Transf., 105, 485–492, 1983.
Van Genuchten, M. T. and Nielsen, D. R.: On describing and predicting the hydraulic properties of unsaturated soils, Ann. Geophys., 3, 615–628, 1985, http://www.ann-geophys.net/3/615/1985/.
Wagner, W. and Pruess, A.: The IAPWS formulation 1995 for the thermodynamic properties of ordinary water substance for general and scientific use, J. Phys. Chem. Ref. Data, 31, 387–535, 2002.
Whitaker, S.: Simultaneous heat, mass and momentum transfer in porous media: a theory of drying, Adv. Heat Trans., 13, 119–203, 1977.
Whitaker, S. and Chou, W. T.-H.: Drying granular porous media – Theory and experiment, Drying Technol., 1, 3–33, 1983–1984.
Yaws, C.: Handbook of Transport Property Data, Gulf Publishing Company, Houston, TX, USA, 1985.

GMDD
8, 2555–2603, 2015

Yoshida, K., Matubayasi, N., and Nakahara, M.: Self-diffusion of supercritical water in extremely low-density region, J. Chem. Phys., 125, 074307, doi:10.1063/1.2333511, 2006.
Yoshida, K., Matubayasi, N., and Nakahara, M.: Erratum: Self-diffusion of supercritical water in extremely low-density region (J. Chem. Phys. 125, 074307, 2006), J. Chem. Phys., 126, 089901, doi:10.1063/1.2372501, 2007.

GMDD
8, 2555–2603, 2015

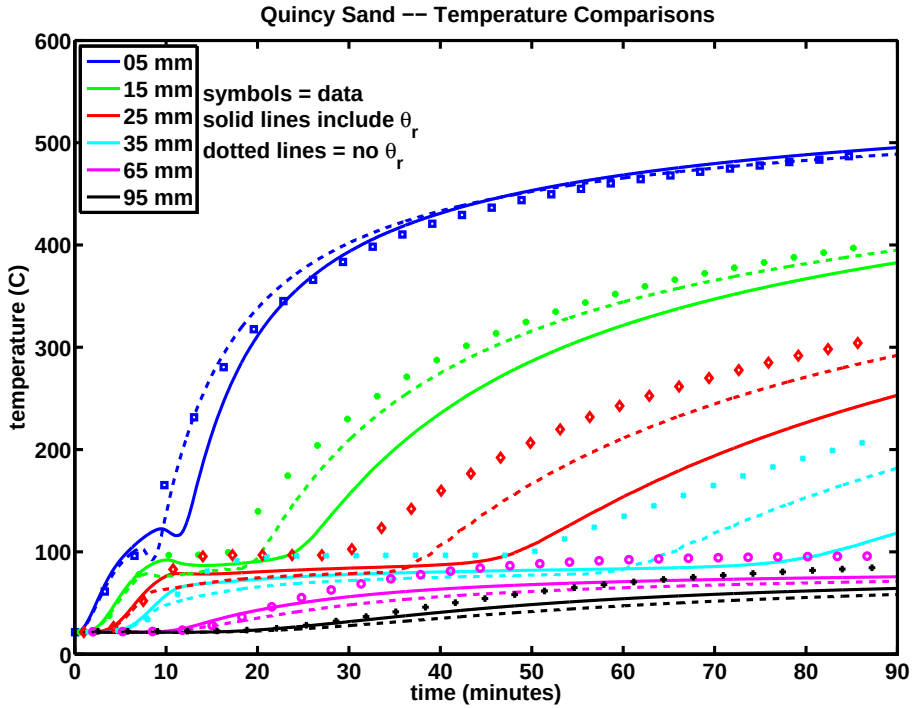

Figure 1. Comparison of measured (symbols) and modeled (lines) soil temperature during the Quincy Sand heating experiment. The solid lines are model simulations that include the dynamic residual soil moisture, θ_r; the dotted lines correspond to simulations that exclude θ_r. To compare with the equilibrium model see Fig. 2 of Massman (2012).

GMDD
8, 2555–2603, 2015

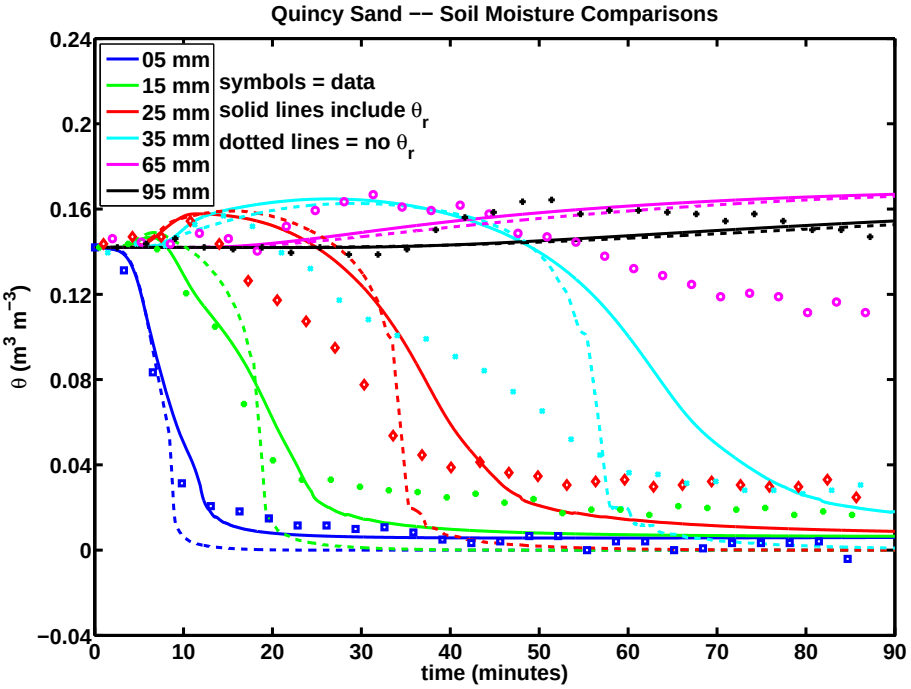

Figure 2. Comparison of measured (symbols) and modeled (lines) soil moisture content during the Quincy Sand heating experiment. The solid lines are model simulations that include the dynamic residual soil moisture, θ_r; the dotted lines correspond to simulations that exclude θ_r. To compare with the equilibrium model see Fig. 3 of Massman (2012).

GMDD
8, 2555–2603, 2015

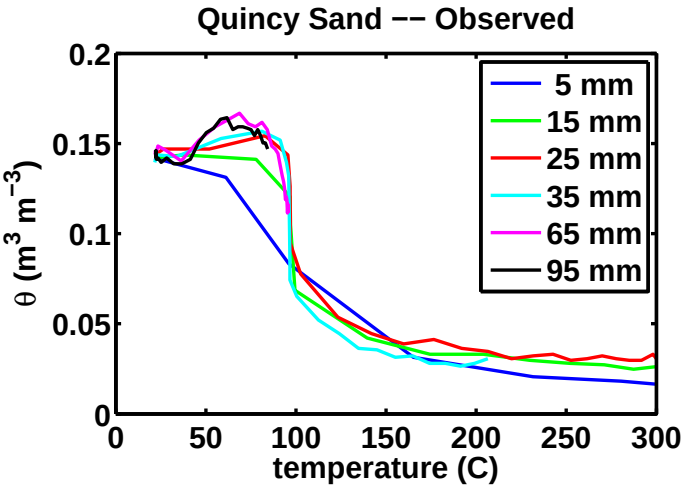

Figure 3. Measured soil moisture vs. measured soil temperatures for the Quincy Sand heating experiment (see previous two figures).

GMDD
8, 2555–2603, 2015

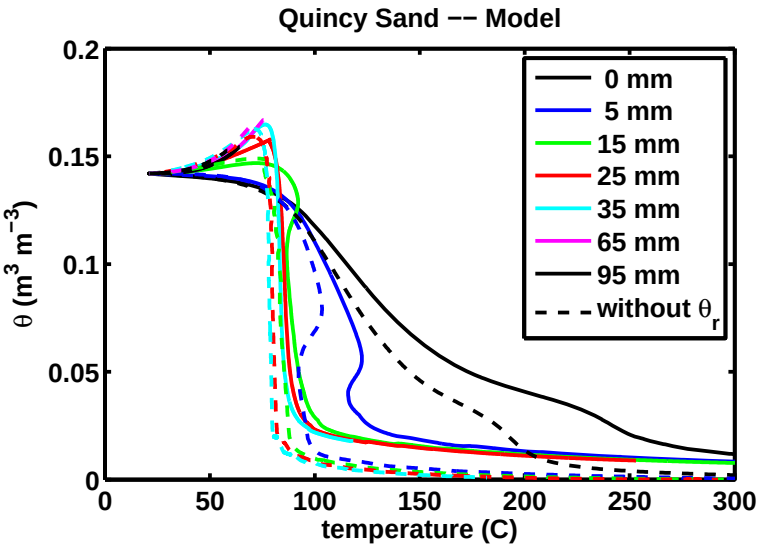

Figure 4. Modeled soil moisture vs. modeled soil temperatures for the Quincy Sand heating experiment (see Figs. 1 and 2 above). The solid lines are model simulations that include the dynamic residual soil moisture, θ_r; the dotted lines correspond to simulations that exclude θ_r. This is the solution space representation of the model solution, which is to be compared with the observations shown in the preceding Fig. 4, as well as with the equilibrium model results shown in Fig. 5 of Massman (2012).

GMDD
8, 2555–2603, 2015

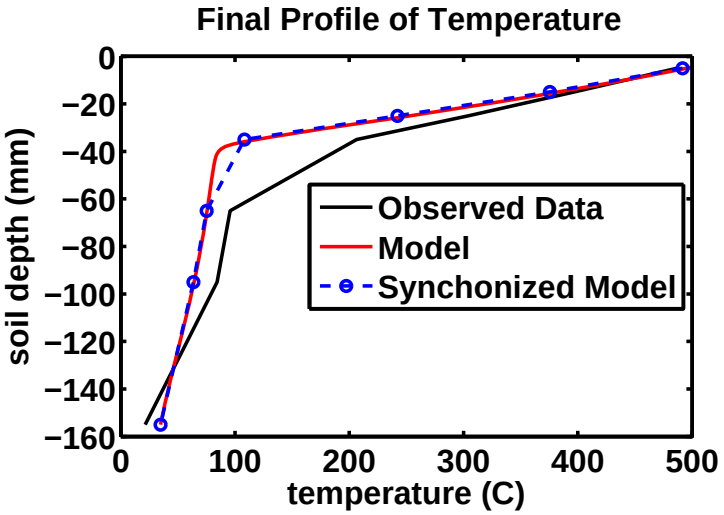

Figure 5. Comparison of the final modeled and measured temperature profiles at the completion of the 90 min Quincy Sand heating experiment. Because the data shown in the measured profile (black) are not precisely coincident in time, the full model results (red) were sub-sampled in synchrony in time (and coincide in space) with the observations. This time-synchronized model profile is shown dashed blue. To compare with the equilibrium model see Fig. 6 of Massman (2012).

GMDD
8, 2555–2603, 2015

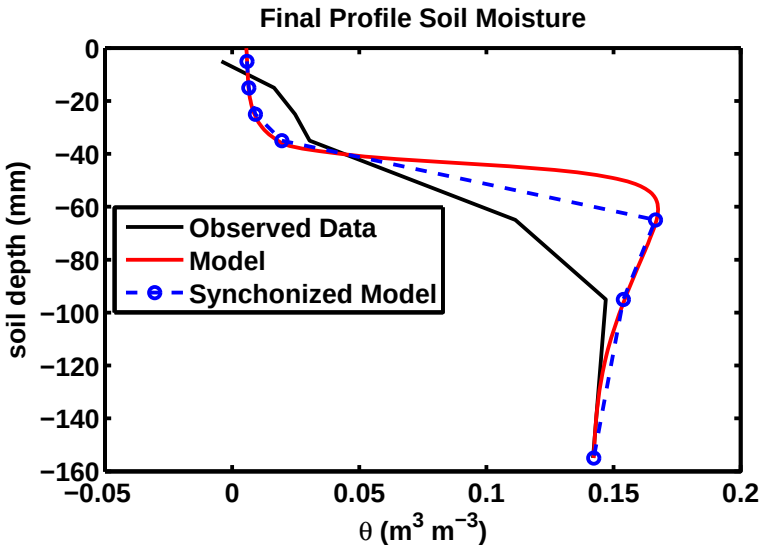

Figure 6. Comparison of the final modeled and measured moisture profiles at the completion of the Quincy Sand heating experiment. Because the data shown in the measured profile (black) are not precisely coincident in time, the full model results (red) were sub-sampled in synchrony in time (and coincide in space) with the observations. This time-synchronized model profile is shown dotted blue. The observed data (black) suggest that the total water lost during the 90 min experiment was 31 % of the initial amount. The model simulation (red) indicated a 20 % loss and the synchronized-model (blue) yielded a 24 % loss. Note the recondensing soil moisture (between 40–60 mm depth) ahead of the drying front. To compare with the equilibrium model see Fig. 7 of Massman (2012).

GMDD
8, 2555–2603, 2015

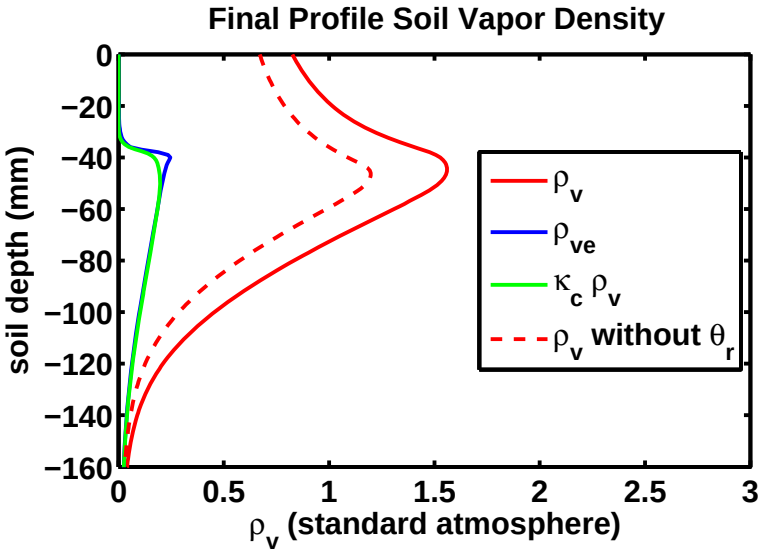

Figure 7. Final modeled profiles of vapor density [ρ_v], equilibrium vapor density [ρ_{ve}], and the condensation coefficient ($\mathcal{K}_c$) modified vapor density term [$\mathcal{K}_c\rho_v$] used with the non-equilibrium model source term, S_v, at the completion of the 90 min model simulation. The solid lines are model simulations that include the dynamic residual soil moisture, θ_r; the dotted lines correspond to simulations that exclude θ_r. The maximum vapor density (for the θ_r case) is about 1.5 times the density of the standard atmosphere (= 1.292 kg m^{-3}) and is located the near the level of maximum evaporation and the level of maximum soil moisture. This figure should be compared with the equilibrium model result: Fig. 8 of Massman (2012).

GMDD
8, 2555–2603, 2015

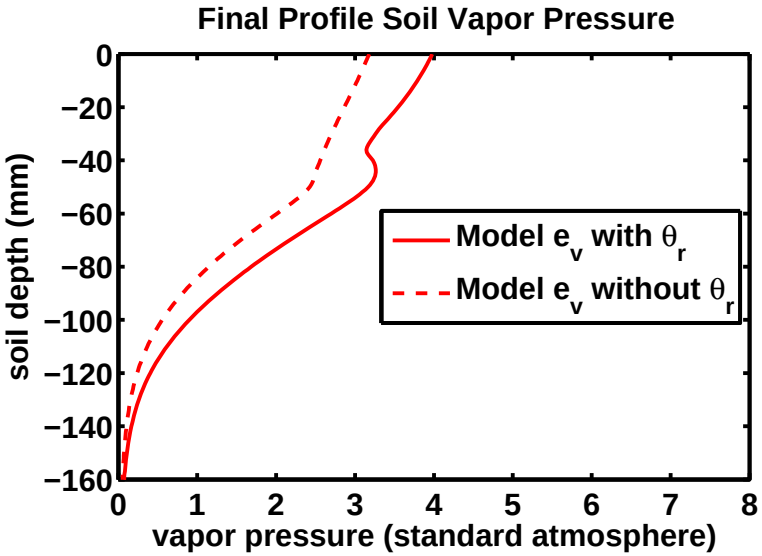

Figure 8. Final modeled profile of vapor pressure at the end of the 90 min model simulation. The solid lines are model simulations that include the dynamic residual soil moisture, θ_r; the dashed lines correspond to simulations that exclude θ_r. In both cases the maximum vapor pressure occurs at the soil surface. For the θ_r case this maximum vapor pressure is about 4 times the pressure of one standard atmosphere (= P_{ST} = 101.325 kPa).

GMDD
8, 2555–2603, 2015